COMPUTATIONAL STUDY USING TENSILE FORCE AND TORQUE TO MANIPULATE AXIAL CHIRALITY IN BIARYL MOLECULES

By

Mathew P. Neal

A thesis submitted to the Department of Chemistry

In conformity with the requirements for

the degree of Master of Science

Queen's University

Kingston, Ontario, Canada

(January, 2017)

ABSTRACT

Biaryl molecules are widely studied systems that have applications in a broad selection of fields including pharmaceuticals, environmental protection, liquid crystal synthesis, and metal organic framework synthesis. Extra care is required in consideration of the axial chirality they often exhibit. Careful control of axial chirality in biaryl molecules is a blossoming area of study which remains open to fresh interpretation. This study, employing quantum chemical calculations and first principles molecular dynamics simulations, has demonstrated that a mechanochemical scheme may be employed wherein mechanical work introduced by the application of tensile forces and torques can be used to promote enantiomeric excess in a number of axially chiral substituted biaryl molecules. Furthermore, quantitative control over the timescales of biphenyl rotation and chiral purification is offered. Subsequently, a system incorporating Taylor series approximations has been employed to approximate the effects of mechanical work on the potential energy surface, reducing the number of quantum chemical calculations required in order to identify a suitable range of tensile forces and torques in order to achieve enantiomeric excess.

Acknowledgements

I would like to acknowledge the following people and organizations for their efforts in the completion of this thesis: Dr. Nicholas Mosey, Dr. Tucker Carrington, and Dr. Natalie Cann; fellow lab members Gurpaul Kochar, Laura Laverdure, Soran Jahangiri and Yaoting Zhang for collaborations and conversations on the topic of mechanochemistry; HPCVL, Compute Canada, and SHARCNET for providing computational resources, and NSERC for financial support; and Queen`s University and the Department of Chemistry for the guidance and opportunity they have provided.

Statement of Originality

I hereby certify that all of the work described within this thesis is the original work of the author. Any published (or unpublished) ideas and/or techniques from the work of others are fully acknowledged in accordance with the standard referencing practices.

(Mathew P. Neal)

(July, 2016)

Table of Contents

List of Figures

List of Tables

List of Acronyms

AFM: Atomic Force Microscopy

CASSCF: Complete Active Space Self-Consistent Field

COGEF: COnstrained Geometries simulate External Force

dof: Degree of Freedom

DFT: Density Functional Theory

EFEI: External Force is Explicitly Included

FMPES: Force-Modified Potential Energy Surface

FPMD: First-principles Molecular Dynamics

GTOs: Gaussian type orbitals

LDA: Local Density Approximation

MD: Molecular Dynamics

NH: Nosé-Hoover

PES: Potential Energy Surface

PPs: Pulling Points

STOs: Slater type orbitals

TS: Transition State

TST: Transition State Theory

QC: Quantum Chemical

FMPES: Force Modified Potential Energy Surface

Chapter 1: Introduction

1.1 Introduction to Mechanochemistry

Mechanochemistry stands alongside electrochemistry, thermochemistry, and photochemistry, as methods for overcoming reaction barriers and facilitating the conversion between reactants and products. Whereas these other methods use electric potentials, thermal energy, or photons to overcome a reaction barrier, mechanochemistry makes use of mechanical forces and work. Mechanochemistry accomplishes this by directing mechanical work along a specific nuclear degree of freedom (dof) associated with the conversion between reactant and product structures, the reaction coordinate. This work lowers the energy barrier which must be overcome to proceed along the reaction coordinate. This is illustrated in figure 1-1.

The origins of mechanochemistry lie in the application of forces to bulk samples of solid material which has evolved into milling as it is known today.[1] Over time the potential of mechanochemistry to influence chemical reactions at a single molecule level has begun to garner interest.[2,3] This interest stems from the tantalizing prospect of controlling reactivity along a specified degree of freedom using mechanical work. A tensile force (F) is applied between two pulling points (PPs) spanning the reaction coordinate. The work applied is the product of F and the change in PPs distance (R). This mechanical work modifies the reaction barrier along the reaction coordinate as illustrated in figure 1-1. The culmination of this is a mechanochemical means of reducing the energy required to overcome the energetic barrier separating reactants and products for a specific reaction.

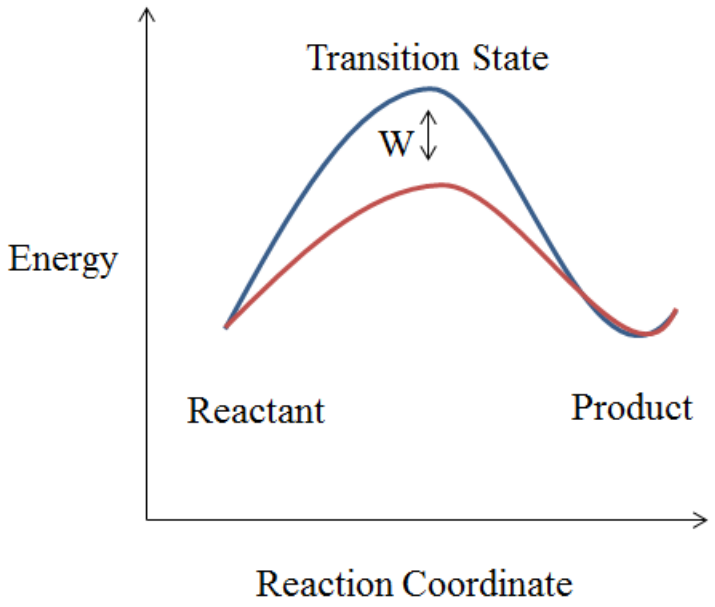

Figure 1-1. The effect of mechanical force and work on a reaction coordinate. The unmodified coordinate is illustrated in blue, and the red represents the reaction coordinate once work has been performed. *W* represents work and reflects the magnitude of difference in energy between the reaction barriers for the modified and unmodified systems. It is worth noting that the energy required for conversion for reactants to products for the modified system is lower when compared to the unmodified system.

1.2 History of Mechanochemistry

One of the first attempts at formally classifying mechanochemistry comes from Wilhelm Ostwald in the 19th century.[4] Ostwald provides a very general description, classifying any chemical or physio-chemical change in aggregate states as mechanochemistry. Specific reference is made to the earliest forms of mechanochemistry, milling and grinding, which have been used since pre-historic times. Experimental mechanochemistry as it is known today was first advocated by

Theophrastus, one of Aristotle's students, who discovered that rubbing cinnabar with brass pestle in a brass mortar with vinegar could be used to produce mercury:

$$HgS + Cu \rightarrow Hg + CuS$$

Mechanochemistry has broadened its applications considerably since the days of Theophrastus. Moving into the twentieth century, mechanochemistry revealed itself as a useful tool for studying the effects of high pressures on the transitions of crystals, as well as the rates of solid-state reactions.[5] Material science applications continued to expand past the mid 1900's as ball mill apparatus were used to produce oxide dispersion strengthened nickel and iron based superalloys. Today this method is called mechanical alloying, and provides an alternative to conventional melting and casting techniques for producing alloys.[6] Ball mill apparatus apply both pressure (perpendicular to surface) and shear (parallel to surface). Manipulation of pressure and shear contribute to the overall versatility of ball mill based mechanochemical activation. Further developments have produced jet mills, turbulent mills, and high peripheral speed mills. These are collectively referred to as shock action apparatus and they apply mechanochemical work by colliding particles with solid surfaces using gas jets or moving blades. Shear action mills have also emerged wherein material is placed between two solid surfaces which are then dragged across each other. The result is a powerful shear force applied to the material caught in-between. This technique has proven useful for the purposes of mechanochemical synthesis.

The methods discussed thus far involve bulk scale production and non-specific application of forces. In the context of activating reactions, it is true that forces are being applied along the reaction coordinate, however many erroneous forces are also being applied along other degrees of freedom, due to the non-specific nature of the ball mill procedure. For many applications, this is

fine; however, for those wishing to investigate mechanochemical activation at a molecular level with a high degree of precision, something is left to be desired. For this reason, mechanochemical advancement in the last few decades has made great strides in terms of how forces can be applied precisely along specific degrees of freedom at the level of a single molecule. Subsection 1.4 of this chapter will focus on methods that are capable of applying work in a precise manner for single molecule systems. This will be followed by suggestions for how precise application of forces may be utilized in a way that is useful for industrial bulk scale applications. In other words, mechanochemical methodology will come full circle back to bulk scale systems, however with the erroneous and non-specific mechanical work removed.

The picture of molecular level mechanochemistry presented thus far mostly incorporates simple tensile forces performing mechanical work over a defined pulling point distance. One significant contribution of this thesis is to introduce the utility of expanding this view of mechanochemistry to incorporate work performed by the product of torque forces (τ) applied over torsional angles (ϕ). In other words, to expand the repertoire of mechanical forces from just simple pushing and pulling towards twisting. Although the full utility of τ in a mechanochemical context still needs broader exploration, manipulation of axial chirality serves as an example of one specific application which is useful for illustrating how τ can be used to open up new kinds of chemistry made uniquely possible by mechanochemistry.

1.3 Axial Chirality

Axial chirality involves the relative orientation of adjacent planes within a molecule (Figure 1-2). Unlike more common examples of chiral molecules, axially chiral systems need not

contain a stereogenic center. Instead, the axially chiral states, referred to as atropisomers, are differentiated by rotation of internal planes about an axis.[7-11]

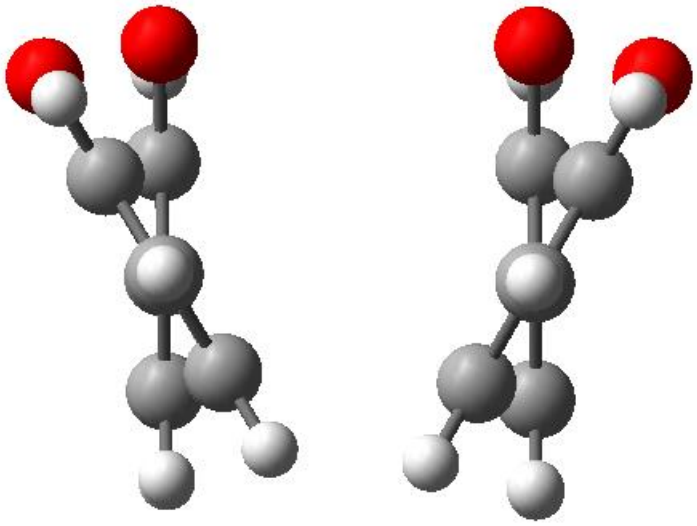

Figure 1-2. Atropisomer forms are presented using a generic representation of a substituted biaryl molecule. These atropisomers are enantiomers with respect to axial chirality. Axial chirality involves the relative orientation of adjacent planes in a molecule, as shown. Fine control of these atropisomers is of significant interest synthetically and pharmacologically.

Biaryl systems such as 2,2'-Bis(diphenylphosphino)-1,1'-binaphthyl (BINAP) are often presented as the prototypical axially chiral systems, and have been used extensively both on a practical and synthetic front due to the strong foundation they provide for interesting synthetic strategies, including medical, pharmacological, and materials applications.[12] Recent experimental work was reported in which a system of axially chiral biaryl molecules was mechanochemically racemized by applying a force F to a pair of substituents in the ortho positions. This was achieved because applying F stabilized the planar transition state (TS) to the point at which it became a minimum energy structure on the potential energy surface (PES). This planar structure serves the role of a prochiral state in which rotation about the central C-C bond can reach either atropisomer.

Releasing F increased the energy of the planar structure relative to the minima on either side of the TS, which correspond to the pair of atropisomers. Since applying F to the ortho groups does not alter the relative energies of the atropisomers, both are formed in equal amounts. Unfortunately, this work has recently been retracted to due to concerns regarding scientific accuracy and ethics, and it is not clear what aspects of that paper are invalid. Nonetheless, calculations performed within our group prior to the retraction of the experimental work have shown that applying F to the ortho positions in biaryls can lower rotational barriers to facilitate the transition between atropisomers. Interestingly, calculations within our group have also revealed that applying F to the para positions in biaryls can also reduce rotational barriers.

In order to achieve enantiomeric excess, it is necessary to change the relative energies of the atropisomers. In the context of mechanochemistry, this can be achieved by applying τ about the central bond of the biaryl. The ability to mechanochemically apply τ has been demonstrated experimentally in a study wherein DNA was unwound using torque applied via molecular tweezers (MT) and monitored with tethered rotating magnetic beads.[13,14] However, until now τ has not been used to tackle problems related to chirality. The application of τ to a biaryl in a manner that affects axial chirality would likely involve the groups in the ortho position. Chapter 3 presents results which indicate that optimized combinations of F applied at the para position and τ at the ortho position in a generic biaryl system show the ability to produce both kinetic and thermodynamic control over the formation of a preferred atropisomer. The specifics of how F and τ differentially affect energies along the reaction coordinate are shown in figure 1-3.

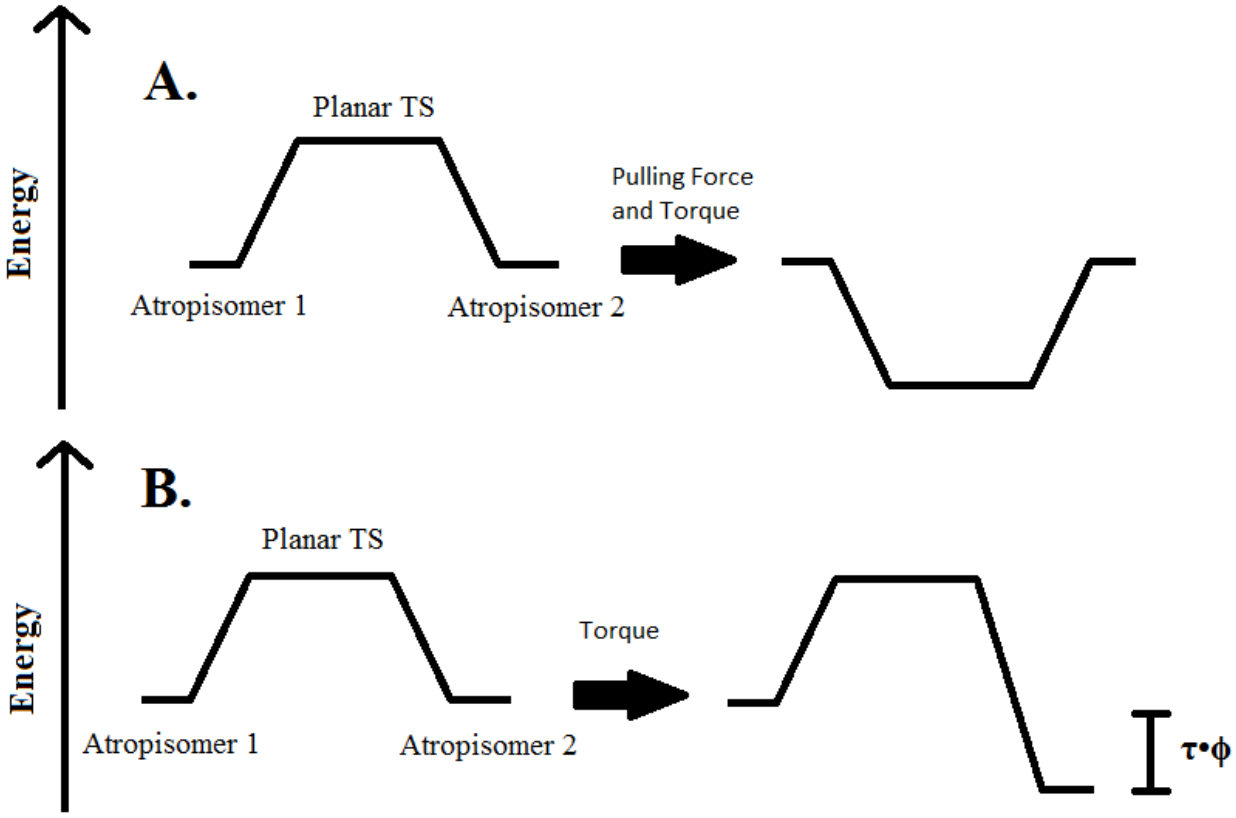

Figure 1-3. The energetic basis of kinetic and thermodynamic effects arising from the work performed on a rotational energy barrier by pulling forces and torques is illustrated. Part A Illustrates how work performed by both pulling forces (F) and torques (τ) contributes to lowering the energy of the rotational barrier separating atropisomers in an axially chiral biaryl system. The barrier is lowered such that it forms a new minimum, representing a force stabilized planar transition state. Part B illustrates the unique effect that τ has in creating an energetic inequality amongst the atropisomers. The work done by τ is rotationally anisotropic, meaning the work performed is unequal across the rotational degree of freedom. This causes a change in the reaction energy of interconversion between atropisomers equal to the work done, which is the product of τ and ϕ where τ is the magnitude of the torque applied and ϕ is the angle of separation between atropisomers.

As stated previously, there have been no experimental attempts at applying τ at the scale of a single biaryl molecule. However, the ability to do so is by no means out of reach. A number of disparate experimental strategies exist which are capable of performing key functions, such as single molecule force applications, application of torques, etc.[13,14] These disparate strategies could be integrated in such a way that single molecule F and τ application could be experimentally performed; enabling a mechanochemical enantioenrichment strategy to be realistically pursued. For this reason, it is pertinent that a review of the relevant contemporary experimental methods be presented.

1.4 **Experimental Mechanochemistry Review**

Atomic force microscopy (AFM) is a single molecule imaging and manipulation technique that has proven particularly powerful in the study of protein folding properties.[15-17] A general schematic for one of these devices is illustrated in figure 1-4. In this technique a sample is fixed on two ends by a cantilever tip and a solid stage. Force is applied to the sample as the cantilever is moved relative to the copper stage. The extent of the cantilever movement, and by extension, the force applied to the sample is measured by the deflection of a laser off the back of the cantilever towards a position-sensitive detector. Deformation of the sample can be modeled using the magnitude of force applied (obtained indirectly through deflection measurements) and the spring constant attributed to the sample. The spring constant depends on the material composition of the sample, but usually falls within the range of 10^1 - 10^5 pN / nm. The range of forces that AFM can apply usually falls within a range of 10^1 - 10^4 pN. It is worth noting that the results presented in chapter 3 were obtained with an upper limit of 2000 pN applied.

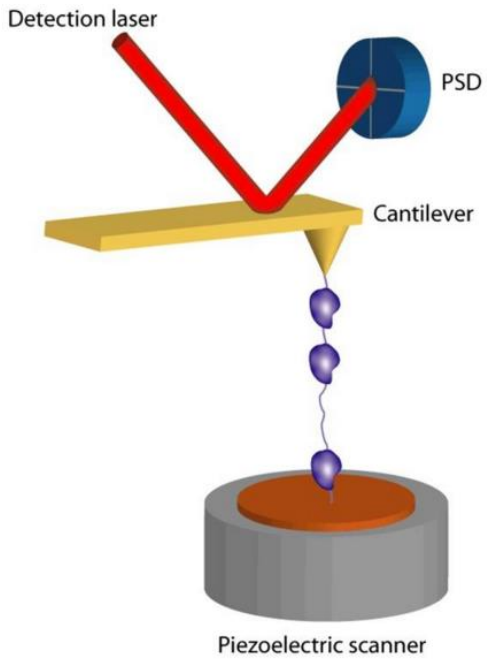

Figure 1-4. Above is illustrated a simplified AFM schematic (not to scale). The sample can be seen as the purple material held between the cantilever tip and the piezoelectric scanner. The orange surface of the scanner represents the surface which directly tethers the sample. The distance between the copper surface and the cantilever tip is controlled by movement of the piezoelectric scanner along the axis formed by the sample. This causes propagating forces which result in movement of the cantilever plate on the other end of the sample, which is measured through cantilever position dependent deflection measurements of the laser towards a position sensitive device (PSD).[18]

Optical tweezers are another experimental tool that was popularized in the 1970's.[19] A single spherical bead is tethered non-covalently to some sample. The bead is optically transparent and is subjected to a focused laser beam which exerts radiation pressure on it and controls its position. When the laser is moved, it transmits a force to the bead proportional to the displacement of the laser. The bead follows the focus of the laser via a restoring force and transmits some of this

to the sample via the non-covalent linker.[17] Conversely, samples which move independently, such as biologically active samples, may pull the bead along with them. In these cases, the bead is moved by the sample, and the movement of the laser to keep up with the bead can be used as a means of measuring the force exerted on the bead by the sample. An example of this is illustrated in figure 1-5 wherein RNA polymerase pulls an optical bead along a strand of DNA whilst laser refocusing is used to measure the forces involved.

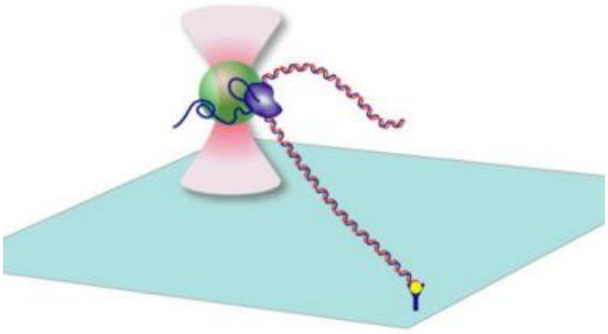

Figure 1-5. An example of an optical tweezer setup is illustrated (not to scale). In this scheme, RNA polymerase pulls an optical bead along a strand of DNA. The restoring forces between the optical bead and the laser are then measured in order to indirectly measure the force exerted on the bead by RNA polymerase. The intent of this particular scheme is for characterization of RNA polymerase, although wildly varying schemes exists attributed to the great flexibility inherent to the optical tweezer method.[20]

The restoring force measured between the moving laser and/or bead is modeled using Hooke's law:

$$F = -k\Delta z \qquad 1.1$$

where F is the magnitude of the restoring force, k is the force constant, and Δz is the displacement of the optical bead from the laser's focus. k is variable with the focal width of the laser, as well as the optical bead's polarizability. Interestingly, force can also be applied to the optical bead not by moving the laser, but by varying it's intensity over time. In this example, the restoring force is uniquely determined by the gradient of the laser intensity with respect to time. Optical tweezers have been used to experimentally apply forces within a range 0.1 – 100 pN. This method is praised for its wide breadth of application, particularly with regards to biological macromolecule manipulation and characterization.[21-24] One such example has already been presented in figure 1-5.

Magnetic tweezers are another experimental technique which allow for the application of twisting forces at a molecular level.[25] These use a superparamagnetic bead suspended in an external magnetic field. The magnetic field exerts a force on the bead which is proportional to the gradient of the field at the location of the superparamagnetic bead. Manipulating the position of the magnets generating the magnetic field provides a means to influence the force applied to the bead. Figure 1-6 shows a scheme wherein magnets are rotated, resulting in a twisting force experienced by the bead which is then propagated to a sample which is tethered to the rotating bead. This technique provides the means of applying torques to molecular scale systems and has been used in experiments wherein biological macromolecules such as DNA and chromatin have been unwound or supercoiled.[13,14]

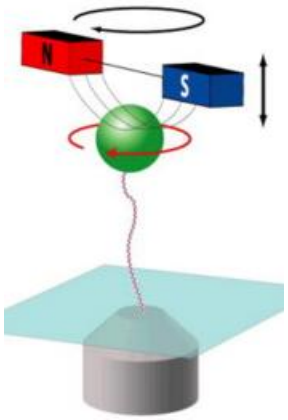

Figure 1-6. A simplified schematic of a magnetic tweezer device (not to scale). The magnetic field produced by the red and blue magnets exerts a force on the superparamagnetic bead (in green) proportional to the gradient of the magnetic field at the location of the bead. The bead is tethered to a sample to which it propagates this force. Movement of the magnets can be used to manipulate the nature and intensity of the force felt by the bead. In the example shown, the magnets are rotated to exert a torque on the bead.[20]

Table 1-1. A comparison between various measurement related properties of the optical tweezers, magnetic tweezers, and atomic force microscopy methods.[20]

	Optical tweezers	Magnetic Tweezers	AFM
Spatial resolution (nm)	0.1-2	5-10	0.5-1
Temporal resolution (s)	10^{-4}	10^{-1}-10^{-2}	10^{-3}
Force range (pN)	0.1-100	10^{-3}-10^{2}	10-10^{4}
Displacement range (nm)	0.1-10^{5}	5-10^{4}	0.5-10^{4}
Probe size (μm)	0.25-5	0.5-5	100-250

AFM, optical tweezers, and magnetic tweezers all confer an experimental opportunity to apply forces in a controlled way at a molecular level. Of particular note are magnetic tweezers, which allow for torques to be applied. The importance of this distinction is highlighted by the sequence of high profile publications from the last decade which have shown marked improvements in control over the torque applied, as well as the systems to which it can be applied. Method variations such as magnetic torque tweezers (MTT) and freely orbiting MT (FOMT) are notable from these publications.[26,27] The current state of the literature demonstrates that the most common use for these techniques is characterization of biological macromolecules such as DNA and chromatin. One hopes that the utility of expanding the scope of these methodologies to apply torques to small molecules within the context of axial chirality will be recognized. One of the goals of the work presented in this thesis is to motivate said recognition.

The ability to apply forces at a molecular scale using the aforementioned methods is attractive from an academic investigative standpoint; however limited throughput makes them unattractive for practical large scale industrial synthetic purposes. One branch of contemporary challenges in mechanochemistry involve up-scaling the ability to apply controlled forces at a molecular level. Presently, one method stands out in its capacity to achieve this: molecular force probes.

Molecular force probes were proposed by Boulatov in 2009, and involve linking a sample molecule to an inert molecular probe.[28] These probes must satisfy three criteria: the probe must be more structurally anisotropic than the functional group to which it is bound, the probe's functional groups and chemical transitions must not interfere with the sample to which it is bound, and lastly probe must allow for the transmission of sufficient restoring forces to the sample.[29] Transition of force form probe to sample occurs through the medium of highly variable linkers. The chemical

composition and length of these linkers affects the magnitude of force that is transmitted to the sample, and therefore manipulation of linker properties provides a necessary tool to manipulate the force applied to the sample. Given the aforementioned probe requirements, stiff stilbene molecules have emerged as an attractive general purpose probe. Stilbene cis-trans isomerization can be photochemically controlled. The utility of this photo-isomerization was shown in a study involving the ring opening of trans-3,4-dimethylcyclobutene (Figure. 1-7). The ring opening of dimethylcyclobutene into either its cis or trans hexadiene products could be directly controlled through photoisomerization of the complexed stilbene.

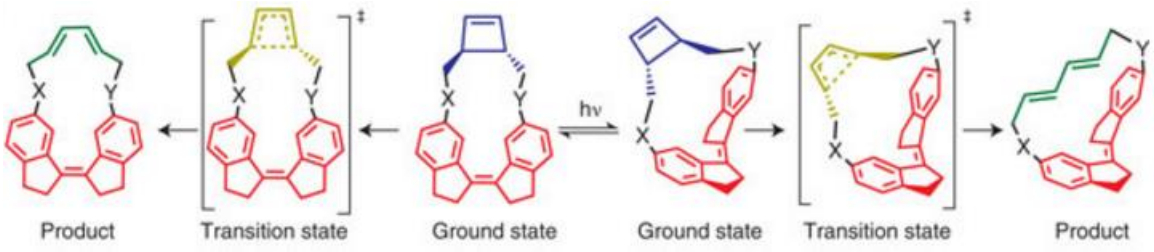

Figure 1-7. Different ring openings of trans-3,4-dimethylcyclobutene. The photoisomerization of the stillben connected to trans-3,4-dimethylcyclobutene by variable linkers X and Y provides the basis for differentiating between the hexadiene products formed. Mechanistically, the restoring forces exerted on trans-3,4-dimethylcyclobutene by the stilbene molecule are responsible for activating the ring opening reaction. The nature of this restoring force depends on the stilbene isomer, which is photochemically controlled. Therefore, photoisomerization of stilbene provides an indirect means of activating one of two parallel trans-3,4-dimethylcyclobutene ring opening reactions.[28]

While molecular force probes provide a tantalizing prospect for the experimental application of forces at an industrially relevant scale, there exist other avenues that bear mention: metal organic frameworks (MOFs). At its first mention, it may seem strange to mention MOFs in

the context of industrial scale experimental mechanochemistry. In fact, the broad applications of MOFs, in conjunction with their preferred methods of synthesis, provide fertile ground for the use of mechanochemistry in producing industrially relevant quantities of homochiral material. Before this can be fully explained, a quick review of MOFs is pertinent.

1.5 Metal Organic Frameworks – Relevance to Mechanochemistry

MOFs, also sometimes referred to as porous coordination polymers (PCPs), are composed of metallic cores (secondary building units – SBUs) coordinated to highly variable organic linker ligands.[29-30] The result is a highly porous complex which can bind a wide variety of small molecule and organic substrates; MOFs have demonstrated aptitude in disparate fields such as material storage, catalysis, and even environmental cleanup. SBU-linker complexes can be functional on their own with substrates bonding directly to the metal core, or several SBUs can be cross-linked by bridging ligands wherein substrates bind to cavities in the functionalized linker topology (Figure 1-8). These multi SBU complexes are more difficult to synthesize, however the complex topology achieved as a result greatly expands the breadth of substrates that may be compatible. Additionally, if homochiral linker ligands are used, it has been shown that asymmetric catalysis can be performed. Recently published work demonstrated that homochiral MOFs achieved asymmetric catalysis of the epoxidation of 2,2-dimethyl-2H-chromene with 71% yield and 82% ee. Areas of difficulty still remain that are common to MOFs as a whole; specifically their instability under conditions of extreme temperatures and their susceptibility to hydrolysis. Fortunately, due to the variable nature of MOFs, specific MOF structures have already been reported which are resistant to these conditions, and have shown competency in normally difficult applications such as heating, cooling, and water absorbant materials. The final difficult consideration when designing MOFs is the response of the cavities to solvent. Before substrate

complexation can occur, solvent molecules must be evacuated from the binding cavities. If the cavities are very large, this evacuation can have substantial effects on the structural integrity of the binding cavity. Unfortunately, the binding cavities are necessarily large for applications involving bio-macromolecules. This results in the need for careful consideration of cavity-solvent interaction for MOF applications involving biological, or otherwise large, substrates.

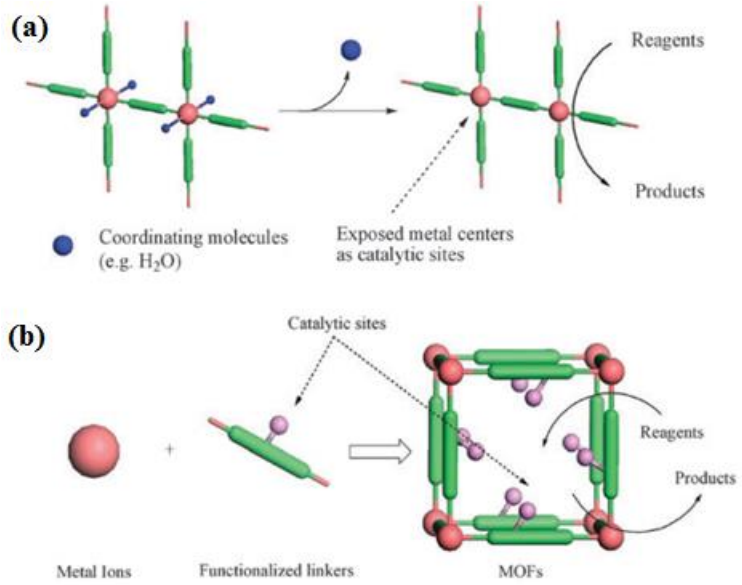

Figure 1-8. Two methods of substrate binding in MOFs are illustrated. Method **(a)** involves binding of substrate to a free coordination site on the metal center of the MOF, once solvent molecules have been displaced. Method **(b)** involves binding of substrate to cavities formed by the topology of functionalized linker ligands that bridge several metal cores.[29]

Relating the idea of MOF asymmetric catalysis back to mechanochemistry requires some understanding of how chiral MOFs are made.[29-30] As mentioned previously, they involve the complexation of a metal core to homochiral bridging linker ligands. The factor that ties mechanochemistry to MOF asymmetric catalysis is the synthesis of these chiral linker ligands. One author states: "Typically, an individual pursuing MOF research spends more than eighty

percent of his/her time performing organic synthesis." The primary burden of this organic synthesis is attributed to the design of new chiral ligands that can be used as building blocks for new MOFs. An example of one such chiral ligand is illustrated in Figure 1-9. Many of these chiral ligands contain centers of axial chirality, most commonly a BINAP derivative. The problem is that homochiral synthesis of a great variety of these axially chiral BINAP-like molecules is cumbersome from the perspective of an organic synthesis approach. This is where the simplicity of a mechanochemical enantioenrichment method demonstrates its use.

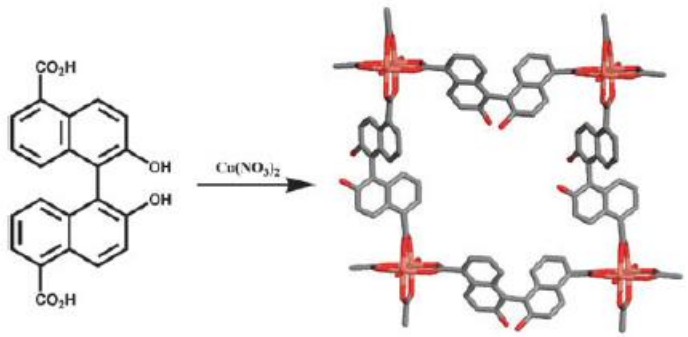

Figure 1-9. An example of a chiral linker ligand that would be used in the formation of a homochiral MOF catalyst for asymmetric synthesis. As can be seen, the linker is a BINAP derivative, and as such possesses axial chirality about the central rotating bond connecting the two aryl groups. On the right can be seen how these linker ligands complex with the metal centers, or SBUs, to ultimately form a complete MOF structure.[29]

Mechanochemistry is capable of biasing the kinetics and thermodynamics of an axially chiral system using mechanical forces which are largely insensitive to chemically active functional group substitutions. This means that a large variety of substituted chiral ligands could be synthesized without the same scaling of difficulty that would be seen in an organic chemistry approach. The downside of experimental mechanochemistry in its present state is the difficulty to upscale it to an industrially relevant scale. In the case of MOFs, however, only a relatively small

amount of the chiral ligands need to be synthesized to produce a homochiral catalyst. This catalyst then imparts its chirality unto the formed product, amplifying the number of chirally pure molecules many fold. To reiterate this idea simply, small scale mechanochemical enantioenrichment can be used to produce chiral ligands, which then are used to synthesize homochiral MOF catalysts which may then amplify the chirality of mechanochemical origin. This overall strategy is even more promising when consideration is taken of the great strides towards rational design of MOF catalysts. Due to advancements in x-ray technology and symmetry-guided MOF design, rational design of MOFs has taken great strides.[30] This means that mechanochemically enantioenriched ligands need not be produced without direction, but rather they may be produced at request as the need arises for the rational design of a MOF catalyst for an emerging application.

1.6 Objectives of thesis

Mechanochemistry has the potential to play an important role in shaping experimental strategies for tackling problems related to axial chirality. These problems touch on a range of important applications: pharmaceuticals, environmental protection, storage of toxic materials and other small molecules. This thesis aims to clearly outline and explain in depth the arguments for using a mechanochemical approach to achieving enantiomeric excess in axially chiral systems. This involves a scheme wherein F and τ are used in combination to predictably alter the kinetics and thermodynamics of rotation about an axis of chirality to favor one atropisomer. The theory and underlying mathematics will be explored. Additionally, a series of calculations involving substituted biaryl molecules will be used as a case study to demonstrate the effectiveness of mechanochemical enantioenrichment. Finally, work that aims to simplify the selection process for F and τ used for enantioenrichment will be presented. This involves a series of numerical

approximations which ultimately remove the need for experimental chemists to perform large numbers of quantum-chemical calculations in order to implement mechanochemical enantioenrichment. Finally, conclusions and imminent challenges will be outlined, with an emphasis on what steps may be taken to move towards realization of experimental mechanochemical enantioenrichment.

Chapter 2 will review the methods and underlying theory. Chapter 3 presents results and discussion focusing on QC calculation and MD simulations demonstrating the possibility of mechanochemical enantioenrichment. Chapter 4 presents results and proposals related to the design of a simplified scheme for predicting F and τ values required to achieve enantiomeric excess – without relying on large numbers of QC calculations. Chapter 5 is dedicated to generating conclusions and discussing the next steps involved in the continuation of this work.

References:

1. Beyer, M.K.; Clausen-Schaumann, H. Chem. Rev. 2005, 105, 2921-2948.
2. Gilman, J.J; Science, 1996, 274, 65.
3. Krüger, D.; Rousseau, R.; Fuchs, H.; Marx, D.; Angew. Chem. Int. Ed. 2003, 42, 2251.
4. Boldyrev, V.V.; Tkáčová, K. J. Mat. Syn. Proc. 2000, 8, 121-132.
5. Bridgeman, P.W.; Rev. Modern. Phys. 1946, 18, 1-93.
6. Suryanarayana, C. Non-Equilibrium Processing of Materials, Pergamon, Oxford, 1999.
7. S.R. LaPlante, P.J. Edwards, L.D. Fader, A. Jakalian, O. Hucke, ChemMedChem 2011, 6, 505.
8. Leroux, F.; ChemBioChem 2004, 5, 644.
9. Pu, L.; Chem. Rev. 1998, 98, 2405.
10. Noyori, R.; Takaya, H.; Acc. Chem. Res. 1990, 23, 345.
11. MacLean, M.W.A. et al., Chem. Mater. 2014, 26, 5852.

12. Leroux, F.; ChemBioChem 2004, 5, 644.

13. Celedon, A. et. al. Nano Lett. 2009, 9, 1720.

14. Gore, J. et. al. 2006, 442, 836.

15. Liang, J.; Fernandez, J. ACS Nano, 2009, 3, 1628.

16. Borgia, A.; Williams, P.M.; Clarke, J. Annu. Rev. Biochem. 2008, 77, 101.

17. Sharma, D.; Cao, Y.; Li, H. Angew. Chem. Int. Ed. 2006, 45, 5633.

18. Neuman, K.C.; Nagy, A. Nature Methods, 2008, 5, 491.

19. Ashkin, A. Phys. Rev. Lett. 1970, 24, 156.

20. Walter, N.G.; Huang, C.Y.; Manzo, A.J.; Sobhy, M.A. Nature Methods, 2008, 5, 475.

21. Kuyper, C.L.; Chiu, D.T. Applied Spectroscopy, 2002, 56, 300A.

22. Ashkin, A.; Dziedzic, J.M. Science, 1987, 235, 1517.

23. deCastro, M.J.; Fondecave, R.M.; Clarke, L.A.; Schmidt, C.F.; Stewart, R.J. Nature Cell. Bio. 2000, 2, 724.

24. Smith, D.E.; Trans, S.J.; Smith, S.B.; Grimes, S.; Anderson, D.L.; Bustamante, C. Nature, 2001, 413, 748.

25. Yan, J.; Skoko, D.; Marko, J.F.; Phys, Rev. E, 2004, 70, 011905.

26. Lipfert, J. et.al. Nat. Commun. 2011, 2, 439.

27. Lipfert J.; Kerssemakers, J.W.J.; Jager, T.; Dekker, N.H.; Nat. Methods 2010, 7, 977.

28.Yang, Q.Z.; Huang, Z.; Kucharski, T.J.; Khvostichenko, D.; Chen, J.; Boulatov, R.; Nature Nanotech. 2009, 4, 302.

29. Ma, L.; Abney, C.; Lin, W.; Chem. Soc. Rev., 2009, 38, 1248.

30. Zhoua, H.; Kitagawa, S.; Chem. Soc. Rev., 2014, 43, 5415.

Chapter 2: Methods

2.1 Introduction

Chemical simulations of o,o'-difluorobiphenyl and various other biaryl derivatives were performed in order to investigate the potential impact of external force, *F*, and external torque, τ, on axial chirality and rotational behavior. Static quantum chemical (QC) calculations were used in conjunction with geometry optimizations and frequency calculations in order to locate and characterize local minima on the force modified potential energy surface (FMPES). The torque contribution to the FMPES was incorporated into existing schemes as part of this work. Analytical and numerical frequency calculations were calculated in a τ dependent manner, and used for cross validation. First Principles Molecular dynamics (FPMD) simulations were performed to further investigate the dynamic nature and behavior of these system subject to ranges of *F* and τ. For these simulations, forces were handled using the External Force Explicitly Included (EFEI) method. Finally, the basis sets and Exchange Correlation (XC) functionals used will be detailed.

2.2 Potential Energy Surfaces

The relationship between atomic/molecular geometry, and energy, is represented by the PES. The PES maps out various structure-energy pairs in 3N – 6 internal degrees of freedom for non-linear molecules (3N – 5 for linear) where N is the number of nuclei in the system. The 6 degrees of freedom lost account for molecular rotational and translational degrees of freedom along 3 Cartesian axes that do not affect internal geometry. The Hamiltonian is the total energy Hermitian operator. Its description is as follows:

$$\hat{\mathrm{H}} = -\sum_{i=1}^{N}\frac{\hbar^2}{2mi}\nabla - \sum_{l=1}^{M}\frac{\hbar^2}{2Ml}\nabla - \sum_{i=1}^{N}\sum_{l=1}^{M}\frac{Z_l e^2}{4\pi\varepsilon_0 r_{il}} + \sum_{i=1}^{N-1}\sum_{j>i}^{N}\frac{e^2}{4\pi\varepsilon_0 r_{ij}} + \sum_{l=1}^{M-1}\sum_{j>i}^{M}\frac{Z_l Z_j}{4\pi\varepsilon_0 r_{lj}} \quad 2.1$$

where N and M are the number of electrons and nuclei respectively, mi and Ml are the masses of the electrons and nuclei respectively, $\hbar$ is the reduced Planck constant (h/2π), ∇^2 is the Laplacian operator, Z_i and Z_j are nuclear charges, e is the charge of an electron, and r_{il}, r_{lj}, and r_{ij} represent electron-nuclear, nuclear nuclear, and electron-electron distances respectively. The first two terms represent kinetic energy of electrons and nuclei in the system. The latter three terms represent nuclear-electron attraction, electron-electron repulsion, and nuclear-nuclear repulsion respectively. Because the mass of nuclei is many orders of magnitude higher than that of electrons, their motions operate on entirely different timescales. Because of this, the movements of electrons and nuclei can be considered separately. This is the basis of the Born-Oppenheimer (BO) approximation, wherein the total wavefunction is separated into nuclear and electronic terms:

$$\Psi_{tot}(\boldsymbol{r}, \boldsymbol{R}) = \Psi_{nucl}(\boldsymbol{R})\Psi_{elec}(\boldsymbol{r}; \boldsymbol{R}) \quad 2.2$$

where **r** and **R** are the electronic and nuclear coordinates respectively. A BO PES can be constructed by solving the electronic Schrödinger equation:

$$\hat{\mathrm{H}}_{elec}\Psi_{elec}(\boldsymbol{r}; \boldsymbol{R}) = E_{elec}\Psi_{elec}(\boldsymbol{r}; \boldsymbol{R}) \quad 2.3$$

where $\hat{H}_{elec}$ is the electronic Hamiltonian operator, and E_{elec} is the electronic energy. Each point on the BO PES corresponds to a different geometry based on permutations of nuclear coordinates along 3N-6(or 3N-5) internal degrees of freedom.[1] Potential energy is calculated for each of these by taking the electronic energy obtained by solving the Schrodinger equation, and adding the nuclear-nuclear repulsion term from equation 2.1. A PES is critical to understanding reactivity. Reactant and product structures can be identified by locating local minima on the PES. These minima correspond to points on the PES where first derivatives are zero (stationary point), and second derivatives along all degrees of freedom are positive. Reactants and products are connected

by a reaction coordinate, which is the degree of freedom providing the lowest energy path connecting reactant to product. Transition state structures can be found at saddle points along the reaction coordinate. A saddle point is characterized by positive second derivatives along all degrees of freedom except for the reaction coordinate, which possesses a negative second derivative.

According to the EFEI formalism, the PES which has been constructed thus far can be modified according to work performed by mechanical forces such as F and τ:

$$\boldsymbol{V}(\boldsymbol{x}, \boldsymbol{F}, \boldsymbol{\tau}) = \boldsymbol{V_{BO}}(\boldsymbol{x}) - \boldsymbol{F}\boldsymbol{q}(\boldsymbol{x}) - \boldsymbol{\tau}\boldsymbol{\phi}(\boldsymbol{x}) \qquad 2.4$$

where $V(\mathbf{x},\boldsymbol{F},\boldsymbol{\tau})$ is the modified potential energy function, V_{BO} is the Born-Oppenheimer (unmodified) potential energy, $\mathbf{x}$ encompasses all nuclear coordinates, $\boldsymbol{F}$ is an external force performed over distance $q(\mathbf{x})$, and $\boldsymbol{\tau}$ is an external torque performed over a torsion $\phi(\mathbf{x})$. In the EFEI approach, external forces are set at fixed values, and the response of molecular geometry to this fixed force is then simulated.

The FMPES can be used to investigate reactivity similar to a regular PES, only now with consideration of mechanical stresses. First and second derivatives can still be calculated on this surface because the mechanical work terms rely on nuclear coordinates as their variables, just as the Born-Oppenheimer energy does. As such, reactant, product, and transition state structures can be identified in systems under mechanical stress of F and τ.

2.3 Effects of External Force on Kinetics and Thermodynamics

The PES can be a very useful tool for extrapolating kinetic and thermodynamic information about reactions. For instance, the change in enthalpy, ΔH, between a reactant-product pair can be used to extrapolate information on the change in Gibbs free energy, ΔG, or change in entropy, ΔS:

$$\Delta H = \Delta G - T\Delta S \tag{2.5}$$

where T is the temperature. The relative change in ΔG from reactant to product can be described:

$$\Delta G(F = 0, \tau = 0) = \Delta G^0 + k_B T ln \frac{[R]}{[P]} \tag{2.6}$$

Where R and P are reactant and product, k_B is the Boltzmann's constant, and ΔG^0 is the standard state free energy change. Once mechanical work performed by external forces is incorporated, the expression becomes:

$$\Delta G(F, \tau) = \Delta G^0 + \frac{k_B T ln[R]}{[P]} - Fq(\boldsymbol{x}) - \tau\phi(\boldsymbol{x}) + \Delta G^{R\to P}_{stretch}(F, \tau) \tag{2.7}$$

where $\Delta G^{R\to P}_{stretch}$ is the change in the relative Gibbs free energy from reactant to product as a result of the movement from a PES to a FMPES.[2] At equilibrium the expression can be simplified:

$$-k_B T ln K_{eq}(F, \tau) = \Delta G^0 - Fq(\boldsymbol{x}) - \tau\phi(\boldsymbol{x}) + \Delta G^{R\to P}_{stretch}(F, \tau) \tag{2.8}$$

where K_{eq} is the equilibrium constant, which is now dependent on F and τ. Reaction kinetics for a general unimolecular reaction can be further be described:

$$\frac{d[P]}{dt} = k[R]^n \tag{2.9}$$

Where R and P represent reactants and products, k is a rate constant, and n accounts for a stoichiometric coefficient. If necessary, k can be calculated using the Arrhenius equation as follows:

$$k = Ae^{\frac{-\Delta E^{\ddagger}}{\mathrm{RT}}} \qquad 2.10$$

where A is the Arrhenius pre-exponential factor, $\Delta E^{\ddagger}$ is the activation energy of a reaction, R is the universal gas constant, and T is temperature. The Arrhenius equation can be used to calculate k when there is a temperature dependence. It makes use of the activation energy which is experimentally determined and related to the reaction barrier.

The effect of external forces on reaction kinetics can also be described. Bell and colleagues described the effect of external tensile force *F* in 1978.[3] A model was constructed to describe observations in cell adhesion. This model proposed that external forces influenced reaction kinetics through lowering of the activation energy:

$$\Delta E^{\ddagger}_{Bell}(F) = \Delta E^{\ddagger}_{0} - Fq(\boldsymbol{x}) \qquad 2.11$$

where $\Delta E^{\ddagger}_{Bell}$ is the reaction barrier energy modified by an external force, F, and $\Delta E^{\ddagger}_{0}$ is the unmodified reaction barrier. This Bell model can easily be extended to include mechanical torques, as well:

$$\Delta E^{\ddagger}_{Bell}(F) = \Delta E^{\ddagger}_{0} - Fq(\boldsymbol{x}) - \ \tau\phi(\boldsymbol{x}) \qquad 2.12$$

A similar approach to explaining the effect of mechanical forces on reaction kinetics was taken 13 years before Bell, by Zhurkov and colleagues.[4] This group proposed a simple model in which the Arrhenius equation was modified in such a way that it could explain observation of mechanical polymer degradation:

$$k(F) = ke^{-(\Delta E_0^{\ddagger} - W)/RT} \quad 2.13$$

Where k(F) is the rate constant dependent on an external force F, and W is the mechanical work performed. Due to the simplicity of using a general work term, this model can be adapted to incorporate torque even more easily than the Bell model:

$$k(F, \tau) = ke^{-(\Delta E_0^{\ddagger} - W)/RT} \quad 2.14$$

where the mechanical work is now dependent on both $Fq(\mathbf{x})$ and $\tau\phi(\mathbf{x})$. In any case, the Zhurkov model explains changes in k in terms of work induced changes in the activation energy of the system.

Other attempts to explain reaction kinetics in this context do so from the point of view of transition state theory (TST).[5] TST necessitates three assumptions: the TS sits on a saddle point along the reaction coordinate, motions of the system around a saddle point can be treated as free translational motion cogent with kinetic theory, and the TS has an associated equilibrium constant which describes its quasi equilibrium state.[6] The equilibrium constant can be formalized:

$$K^{\ddagger} = \frac{[TS]^{\ddagger}}{[R]} \quad 2.15$$

where $K^{\ddagger}$ is the equilibrium constant at the TS, and [R] is the reactant concentration, and $[TS]^{\ddagger}$ is the transition state concentration. This can be expanded upon to describe the rate of product formation:

$$\frac{\boldsymbol{d[P]}}{\boldsymbol{dt}} = \boldsymbol{k^{\ddagger}[TS] = k^{\ddagger}K^{\ddagger}[R]} \quad 2.16$$

where $\frac{\boldsymbol{d[P]}}{\boldsymbol{dt}}$ is the rate of formation of product, and $k^{\ddagger}$ is the rate constant for the conversion between TS species and product. Additionally, $k^{\ddagger}$ is proportional to the vibrational mode that spans the space between TS and product:

$$\boldsymbol{k^{\ddagger} = \kappa\nu} \quad 2.17$$

where ν is the aforementioned vibrational mode and κ is it's corresponding proportionality constant. $K^{\ddagger}$ can be evaluated through its relation to the Gibbs free energy:

$$\boldsymbol{K^{\ddagger}} = \frac{\boldsymbol{k_B T}}{\boldsymbol{h\nu}} \boldsymbol{e}^{\frac{-\Delta \boldsymbol{G}^{\ddagger}}{\boldsymbol{RT}}} \tag{2.18}$$

where $\Delta G^{\ddagger}$ is the Gibbs free energy barrier. By factoring the extended descriptions of $k^{\ddagger}$ and $K^{\ddagger}$ into Eq.(2.16) a new expression is formed for the overall rate constant:

$$\boldsymbol{k} = \boldsymbol{k}^{\ddagger}\mathbf{K}^{\ddagger} = \kappa \frac{\boldsymbol{k_B T}}{\boldsymbol{h}} \boldsymbol{e}^{\frac{-\Delta \boldsymbol{G}^{\ddagger}}{\boldsymbol{RT}}} \tag{2.19}$$

This model is responsive to force modification through its reliance on Gibbs free energy. As explained earlier, external forces have the ability to shift stationary points, including reactant, product, and transition state structures, along the Gibbs free energy surface. This may have the effect of altering the Gibbs free energy barrier, which in turn has a feedback effect on k. If a decrease in $\Delta G^{\ddagger}$ can be instigated by external forces, k is increased, ultimately increasing the rate of reaction. This relationship can be further broken down by sub-factoring $\Delta G^{\ddagger}$ into its enthalpic and entropic components:

$$\boldsymbol{k} = \boldsymbol{k}^{\ddagger}\mathbf{K}^{\ddagger} = \kappa \frac{\boldsymbol{k_B T}}{\boldsymbol{h}} \boldsymbol{e}^{\frac{-\Delta \boldsymbol{S}}{\boldsymbol{R}}} \boldsymbol{e}^{\frac{-\Delta \boldsymbol{H}^{\ddagger}}{\boldsymbol{RT}}} \tag{2.20}$$

This is useful because in TST it is assumed that entropic changes are insignificant relative to their enthalpic counterpart. Fortunately, enthalpic changes closely resemble changes on a potential energy surface, providing good compatibility with models involving a FMPES.

The various kinetic models presented all show a demonstrable relationship between reaction energy barriers, and reaction kinetics. It is through this relationship that this thesis proposes the activation of reactive events across rotational reaction coordinates by lowering rotation barriers mechanochemically using F and τ.

2.4 Geometry Optimizations and Frequency Calculations

The thermodynamic and kinetic properties of chemical systems that can be elucidated as described Section 2.3 rely on knowledge of reactant, product and TS structures. These structures lie on stationary points of the PES; these are points in which the forces (first derivatives) acting on nuclei along all internal degrees of freedom are zero for a specific geometry. Further importance is derived from being able to identify the geometries and associated energies on a PES of stationary points in that they provide necessary information for reaction mechanisms and molecular properties to be inferred. Fortunately, stationary points can be located and characterized by performing nearly ubiquitous techniques in modern computational chemistry: geometry optimizations and frequency calculations.

A geometry optimization is initiated with a starting structure. This can represent a reactant, product or transition state and is little more than an educated starting guess as to the molecular geometry. With this as a starting point, the nuclear coordinates are updated in an iterative process until the condition that forces acting along all nuclei across all internal degrees of freedom are zero (or at least sufficiently close to zero, according to a pre-defined cutoff).[7] It is worth noting that this cutoff often lies in the range of 4.5 x 10^{-4} Hartree / Bohr. One commonly used optimization procedure is the Newton-Raphson method[8]:

$$q_{i+1} = q_i - H_i^{-1} g_i \qquad 2.21$$

where q_{i+1} and q_i are the nuclear coordinates of iteration i+1 and i respectively, g_i contains the first derivatives of energy with respect to changes along 3N degrees of freedom, and H^{-1} is the inverse of the Hessian matrix which contains second derivatives of energy and therefore has dimension 3N x 3N. Elements of g_i are easily calculated, and can be done analytically. Elements of the

Hessian, however, are more costly to calculate with analytical means, and are often approximated numerically alongside the geometry optimization process. With each iteration of q_i, the Hessian is updated as follows:

$$\left(\frac{\partial^2 E}{\partial q_a \, \partial q_b}\right)_i \cong \frac{\Delta\left(\partial E / \partial q_b\right)_i}{\Delta q_a} \qquad 2.22$$

Where $\boldsymbol{\partial} q_a$ and $\boldsymbol{\partial} q_b$ represent partial derivative changes of coordinates q along degrees of freedom a and b respectively within a limit of 3N. These calculations are performed at each iteration until convergence is achieved according to the specified criteria described earlier. Geometry optimizations were used in this thesis in order to obtain reactant, product, and TS structures, and to evaluate changes in the energy of these structures (and their related barriers) between BO PES's and FMPES's.

Frequency calculations corresponding to vibrational degrees of freedom are performed at stationary points for purposes of characterization, and to obtain useful molecular properties. For example, zero-point energies can be evaluated, as well as first order approximations to vibrational partition functions. Calculating vibration frequency involves separating the nuclear Hessian into components of vibrational normal modes (vibrational eigenmodes) and force constants:

$$H = PKP^{-1} \qquad 2.23$$

Where P is a square matrix composed of vibrational eigenmode column vectors, and K is a diagonal matrix with elements containing eigenvalue force constants, k. These eigenvalues can be related to the vibrational frequencies by invoking a diatomic harmonic oscillator approximation:

$$v = \frac{1}{2\pi}\left(\frac{k}{\mu}\right)^{\frac{1}{2}} \qquad 2.24$$

where μ is the reduced mass of the nuclei involved in the vibrational mode, and v is the frequency. Obtaining the k values for a system at a stationary point is useful for purposes of characterization as a local minima, or a TS. If the stationary point is a minimum, then all values of k will be positive for all calculated frequencies. Alternatively, a first order saddle point as a TS can be identified because one of the k values will be negative – the one associated with the reaction coordinate. This in turn results in an imaginary frequency associated with that vibrational mode. Characterization in this way of stationary points on a PES or FMPES is essential to properly map out the correct sequence of reactants, intermediates, transition states and products along a reaction coordinate.

2.5 Incorporating τ into Existing Software

A portion of this thesis was dedicated to updating existing static calculation methods with the capacity to properly incorporate τ induced effects. The largest undertaking as part of this effort involved calculating a Hessian matrix sensitive to τ, for purposes of characterizing stationary points as described above. This involved calculating second derivatives of the τ induced work term on a FMPES. This was done first analytically and then numerically for validation purposes.

Second derivatives were calculated analytically using Tinker code as a guideline.[9,10] Forces applied along a torsional degree of freedom needed to be re-expressed in terms of Cartesian components of forces acting on four torsional atoms. This is required for corrections to be made to the 3N x 3N Hessian matrix. These changes reflect the effects of externally applied forces. First a series of vectors were defined that connected four torsional atoms. Cross products of these vectors were then calculated in order to general torsional planes. The dot product of these cross product vectors was then evaluated in order to relate the torsion angle to the atomic coordinates of

the torsional atoms which were used to define the vectors which constituted the cross product expressions.

Second derivatives were calculated numerically following a central second order finite differences approach:

$$f''(x) \cong \frac{f(x+h)-2f(x)+f(x-h)}{h^2} \quad 2.25$$

as h approaches 0. Elements of the Hessian matrix calculated numerically and analytically were compared in an ethane test system to verify agreement. Agreement was deemed sufficient when the calculated values agreed up to 4 significant figures.

2.6 Molecular Dynamics Simulations

Static calculations are useful for mapping out stable species and reactive intermediates on a PES, however there are inherent limitations. For one, static calculations provide no sense as to the dynamically unfolding nature of the system during reactive events. They provide snapshots of priority structures along a reaction coordinate, but do not give a meaningful sense of how the system behaves in real time. For this purpose, MD simulations are useful. MD simulations provide changes in nuclear coordinates of a system in a time dependent manner through a reactive event. This is achieved by treating the nuclei as classical particles, subject to Newton's equations of motion:

$$\boldsymbol{F}_i = m_i \boldsymbol{a}_i = -\frac{\delta \boldsymbol{V}}{\delta \boldsymbol{r}_i} \quad 2.26$$

Where **F**, **m**, **a**, and **r** are the force, mass, acceleration, and position of nuclei i. V is potential energy of the system, and can be calculated either using force field methods, or in an *ab initio* sense, using quantum chemical calculations. This thesis uses the latter approach.

Integration of the forces yields trajectories for nuclei which in turn update their coordinates over the course of a simulation with some finite number of time steps. It is possible to solve this exactly for systems of two atoms, however for anything larger numerical approximations must be utilized. One such approximation method is the Verlet Algorithm, which approximates changes in nuclear coordinates as follows:

$$\boldsymbol{r}_i(t + \Delta t) = 2\boldsymbol{r_i}(t) - \boldsymbol{r}_i(t - \Delta t) + \boldsymbol{a}_i(t)\Delta t^2 \qquad 2.27$$

Where Δt is a fixed value and represents the time step of the simulation. This approximation has been formulated in such a way that velocities do not need to be calculated directly as part of the algorithm (the integration terms containing velocity cancel by virtue of how the systems properties are updated between time steps). Instead, they are calculated on the side, numerically, simply by taking differences in atomic positions.

$$\boldsymbol{v}_i(t) = \frac{\boldsymbol{r_i}(t+\Delta t) - \boldsymbol{r}_i(t-\Delta t)}{2\Delta t} \qquad 2.28$$

It is important to calculate velocities in order to evaluate the evolution of the systems temperature and energy over the course of the simulation. The fact that velocity and nuclear coordinates are calculated separately complicates the evaluation of these parameters, and for this reason the velocity Verlet algorithm is generally preferred, wherein velocities are updated alongside the nuclear coordinates:

$$\boldsymbol{r}_i(t + \Delta t) = \boldsymbol{r_i}(t) + \boldsymbol{v_i}(t)\Delta t + 0.5\boldsymbol{a_i}(t)\Delta t^2 \qquad 2.29$$

$$\boldsymbol{v_i}(t + \Delta t) = \boldsymbol{v_i}(t) + 0.5\big(\boldsymbol{a_i}(t) + \boldsymbol{a_i}(t + \Delta t)\big)\Delta t \quad 2.30$$

The algorithm requires a starting structure, as well as initial velocities. A starting structure can be easily obtained from literature sources or a geometry optimization. The initial velocities are assigned according to a Maxwell-Boltzmann distribution:

$$f(v) = \left(\frac{m}{2\pi k_B T}\right)^{\frac{3}{2}} \exp\left(-\frac{\frac{1}{2}mv^2}{k_B T}\right) \quad 2.31$$

Extra care must be taken to make sure that the initial velocities coincide with a realistic temperature for the system. If this is not the case after the velocities are initially assigned, then another step is taken to uniformly re-scale the velocities so that they are closer to a target temperature which has been specified. Re-scaling follows the scheme:

$$\boldsymbol{v}_i^{rescaled} = \boldsymbol{v}_i^{orig}\sqrt{\frac{T_{target}}{T_{current}}} \quad 2.32$$

where T_{target} is the desired temperature, and $T_{current}$ is the current temperature which requires correction. Alternative methods of temperature modulation exist, some of which do not impose velocity rescaling uniformly upon all velocity vectors. Many kinds of thermostats exist: Berendsen[11], Anderson[12], and Nosé-Hoover (NH)[13,14] are some of the more common ones. A NH thermostat was used for the MD simulations performed for this thesis. The NH thermostat couples the system to a "heat bath" which is able to freely exchange heat with the system. This resulting distribution of velocities can then be understood statistically within the context of the extensively studied canonical ensemble. Additionally, the extent of heat exchange between the system and the heat bath can be controlled by a mass parameter Q. This mass does not represent any real species in the system, and is introduced as a fictitious mass to be used as an exchange parameter. After

suitable values have been chosen, and the velocities have been rescaled within acceptable parameters, the system is given time to equilibrate. During equilibration the volume (V), number of particles (N), and the temperature (T) are set as fixed parameters. This is referred to as the canonical NVT ensemble (NVT). After equilibration, the behavior of the system is ready to be studied under the effects of some perturbation. 5 picosecond simulations were performed under the Carr-Parrinello formalism on o,o'-difluorobiphenyl subject to F and τ within a range of 2000 pN and 200 pNÅ respectively. The time step (ts) used was carefully chosen so as to make the calculations practical from the standpoint of computational cost, while also not compromising the quality of the results by introducing error in the form of extra energy added to the system. In general, larger ts values result in lower calculation cost at the expense of introducing erroneous energy to the system. A ts value of 6 a.u. was chosen along with a fictitious electronic mass of 400.0 a.u. and a pbe96 exchange-correlation (XC) functional, showing a conservation of the Car-Parrinello Hamiltonian of at least 1.0×10^{-5} Hartree/ps.

2.7 Molecular Orbitals and Basis Sets

Molecular orbitals (MO) can be approximated as a linear combination of basis functions. This linear combination of basis functions is collectively referred to as the basis set. This approximation has proven invaluable for *ab initio* efforts to solve the Schrödinger equation and obtain the total energy of a system. Molecular orbitals are expanded as follows:

$$\chi_i(\boldsymbol{x}) = g(w) \sum_{v=1}^{k} c_{vi} \phi_v(\boldsymbol{r}) \qquad 2.33$$

Where χ_i is a function representing the i^{th} MO, g(w) is the spin function introduced to add the necessary spin, w, to each orbital, and $\phi_v(r)$ are k basis functions with weight factors c_{vi}. The variable r represents orbital spatial coordinates. χ_i can be approximated more accurately with larger

k, a larger number of basis functions per MO. Larger values of k also increase computational cost, however, creating an expected tradeoff of accuracy and computational cost. The MD calculations performed in this thesis made use of plane-wave basis functions. These basis functions are periodic functions and are useful for systems with periodic boundary conditions, common in MD simulations. The static calculations made use of atom centered basis functions of which there are two major types: slater-type orbitals (STO)[15], and Gaussian type orbitals (GTO)[16].

Slater type orbitals can be expressed as follows:

$$\phi_{\varsigma,n,l,m}(r,\theta,\gamma) = NY_{l,m}(\theta,\gamma)r^{n-1}e^{-\varsigma r} \quad 2.34$$

Where N is for normalization, $Y_{l,m}$ are spherical harmonics, ς is an adjustable parameter, r is the distance between the electron and a nucleus, and n, l, and m are the principal, angular momentum, and magnetic quantum numbers respectively. Trends apparent in a slater type orbital have excellent agreement with the exact MOs for the hydrogen atom. For instance, they scale exponentially with r, and possess a cusp at the nucleus. Unfortunately, using a basis set of STOs is difficult, as the product of STOs cannot be integrated analytically.

GTOs can be integrated analytically, making them more computationally practical. In polar coordinates they can be expressed:

$$\phi_{\varsigma,n,l,m}(r,\theta,\gamma) = NY_{l,m}(\theta,\gamma)\sum_{;=1}^{M} r^{l}\left(\frac{2\varsigma_l}{\pi}\right)^{\frac{3}{4}} e^{-\varsigma r^2} \quad 2.35$$

The relationship between GTOs and r is now exponentially squared, implying it decays too quickly as r increases. Additionally, GTOs lack a cusp at the nucleus. In general, they are less effective descriptors at values of r that are very large, or very small, as compared to STOs. Luckily, the description offered by GTOs can be improved by using contracted Gaussian functions, which are

a linear combination of many primitive Gaussian functions.[17] This layer of abstraction provides the means to tweak the shape of a Gaussian function to make it more closely resemble a STO, while still being integratable analytically.

2.8 Density Functional Theory

Density functional theory (DFT) remains the favorite computational method for approximating the multi-electron wavefunction when a balance of cost and accuracy is preferred. Due to its unique approach, it even boasts decreased cost and higher accuracy when compared to some of its older alternatives, such as Hartree Fock; sidesteps of the usual cost-accuracy tradeoff are usually unheard of.[18] DFT introduces the central idea of electron density, which is related to the sought after wavefunction.

$$\rho(\boldsymbol{r}) = N \int \dots \int |\Psi(r)|^2 d\omega dx_1 dx_2 \dots dx_N \qquad 2.36$$

Where $\rho(\boldsymbol{r})$ is the electron density in terms of Cartesian coordinates **r**, N is the number of electrons in the system, and $d\omega$, dx_N are spin and spatial coordinates respectively for said electrons. Whereas the wavefunction relies on 4N coordinates for its description, the electron density only requires three coordinates.[19]

The foundation of DFT lies in the assertion that the energy of a system is related to its electron density in the ground state. This idea is captured in the first Hohenberg-Kohn theorem.[20] The asserted relationship between energy and electron density is formalized by representing the ground-state energy as a function that takes electron density as its input. The energy is then further subdivided as follows:

$$E[\rho] = T[\rho] + E_{ne}[\rho] + E_{ee}[\rho] \qquad 2.37$$

Where $T[\rho]$ is the electron kinetic energy, $E_{ne}[\rho]$ is the nuclear-electron potential energy, and $E_{ee}[\rho]$ is the electron-electron potential energy. Both potential energy terms can be further described:

$$E_{ne}[\rho] = -\sum_I \int \frac{Z_I \rho(\boldsymbol{r})}{|\boldsymbol{R_I} - \boldsymbol{r}|} d\boldsymbol{r} \quad 2.38$$

where Z is the nuclear charge, indexed over atom I with coordinates R.

$$E_{ee}^{classical}[\rho] = \frac{1}{2} \int \int \frac{\rho(\boldsymbol{r_1})\rho(\boldsymbol{r_2})}{|\boldsymbol{r_1} - \boldsymbol{r_2}|} d\boldsymbol{r_1} d\boldsymbol{r_2} \quad 2.39$$

where **r** represent electron coordinates. This term is used to calculate an average electron-electron repulsion throughout the system, however it does not account for more complex non-classical electron-electron interactions such as exchange and correlation. A non-classical correction term must be introduced to account for this.

Thomas-Fermi proposed one of the earliest methods for modeling the kinetic energy term.[21,22] He proposed that the kinetic energy be expressed as a functional of electron density, representing the system as a cloud of non-interacting electron gas. In doing so, it is imposed that the system is a uniform ideal gas – a restriction that limits the theory's practical applicability. There are also the usual limitations inherent to viewing electrons as a uniform gas, namely that quantum effects such as exchange and correlation are ignored. An alternative approach was proposed by Kohn and Sham, who suggested using a wavefunction to calculate the kinetic energy term, rather than electron density.[23] This wave function would be constructed as a Slater determinant of one-electron orbitals, appropriately named Kohn-Sham (KS) orbitals. These non-interacting KS orbitals can be related to the electron density as follows:

$$\rho(r) = \sum_{i=1}^{N} \chi_i^*(\boldsymbol{r})\, \chi_i(\boldsymbol{r}) \quad 2.40$$

where i is one of N total electrons, and χ_i are KS orbitals associated with electron i. Thus, the kinetic energy term, formerly in terms of electron density, can now be expressed in terms of KS orbitals:

$$T_{rs} = \sum_{i=1}^{N} \int \chi_i^*(r) \left(\frac{-\nabla_i^2}{2}\right) \chi_i(r) dr \qquad 2.41$$

where T_{rs} an approximation of the kinetic energy using a reference system described by KS orbitals. The exact kinetic energy can be obtained by introducing a correction term to account for approximations imposed by the KS model.

$$T_{exact}[\rho] = T_{rs}[\rho] + \Delta T[\rho] \qquad 2.42$$

where $\Delta T[\rho]$ is a correction term used to account for imperfections introduced by a KS wavefunction dependent T_{rs} description of kinetic energy. Eq. (2.38) can be rewritten in terms of Eq. (2.40) and Eq. (2.43):

$$E[\rho] = T_{rs}[\rho] + E_{ne}[\rho] + E_{ee}^{classical}[\rho] + E_{ee}^{non-class}[\rho] + \Delta T[\rho] \qquad 2.43$$

where $E_{ee}^{non-class}[\rho]$ is introduced to account for the lack of any non-classical description of electron-electron interactions present in the $E_{ee}^{classical}[\rho]$ term. Eq. (2.44) is very powerful because it offers an exact description of energy in terms of electron density; however in practice this is not attainable because the latter two correction terms cannot be calculated exactly. These correction terms are grouped into what is called an exchange-correlation (XC) functional, $E_{XC}[\rho]$. Eq. (2.44) can be rewritten in terms of the XC functional:

$$E[\rho] = T_{rs}[\rho] + E_{ne}[\rho] + E_{ee}^{classical}[\rho] + E_{XC}[\rho] \qquad 2.44$$

Method improvements for approximating E_{XC} are a large focus of modern DFT development.[24-29] In terms of increasing complexity, the most common kinds of E_{XC} functionals are as follows: Local Density Approximation (LDA)[30,31], Generalized Gradient Approximation (GGA),[32] and Hybrid[33-38]. LDA uses a simple description of electrons as a uniformly distributed charged gas. Their use is popular in some applications, such as solid state chemistry, however for the most part this description is too simple to properly describe the majority of chemical systems.

A more complete view considers local changes in the electron density. This involves incorporating gradients of the electron density into the functional's description of the system. This is the general approach of GGA functionals.[32] The newfound ability to describe changes in electron density greatly expands the scope of systems that can be described with GGA, relative to LDA. GGA still struggles to describe electron exchange interactions, however. To address this, terms can be added to a GGA functional that introduce a HF description of electron exchange. This is effective because HF theory provides an exact description of electron exchange. GGA functionals that incorporate a HF description of exact electron exchange are referred to as hybrid functionals.[33-38] In addition to the above mentioned varieties of E_{XC}, functionals may also have some of their parameters fit to experimental results; these are referred to as semi-empirical functionals. Semi-empirical functionals are often good at reproducing experimental results in systems that are similar to those from which the functionals parameters were fit. However, some criticisms stem from the fact that these functionals may not extent well to exotic systems, as well as the fact that the incorporation of experimental data means that the functional is no longer mathematically "pure". A popular functional which is both hybrid and semi-empirical is B3LYP; it uses Becke's exchange energy[39], and correlation energy provided by Lee, Yang, and Parker. [40]

The E_{XC} functional used in this study was the PBE functional[41], which is a GGA functional that is not fit to any experimental parameters. The reason that this functional was chosen over the very popular B3LYP is because of the planewave basis sets used for dynamics simulations[42]. Hybrid functionals like B3LYP work well with atom centered basis functions; however they produce a singularity during certain convergence steps when planewave basis sets are used. In order to preserve as much consistency as possible (ie. being consistent with E_{XC} usage) between the static QC calculations and the dynamics simulations, a functional needed to be used that was compatible with planewave basis sets, and therefore not Hybrid. PBE was chosen as popular non-hybrid functional.

References:

1. Jensen, F. Introduction to Computational Chemistry, 1999, Wiley, Chichester, England.
2. Bustamante, C.; Chemla, Y.R.; Forde, N.R.; Izhaky, D. Annu. Rev, Biochem. 2004, 73, 705.
3. Bell, G.I. Science, 1978, 200, 618.
4. Zhurkov, S.N. Intern. J. Fracture Mech. 1965, 1, 311.
5. Erying, H. J. Chem. Phys. 1935, 3, 107.
6. Laidler, K.; King, C. J. Phys. Chem. 1983, 87, 2657.
7. Ramachandran, K.I.; Deepa, G.; Namboori, K. Computational Chemistry and Molecular.
8. Ypma, J. T. SIAM Review, 1995, 37, 531.
9. Shi, Y., et al., J. Chem. Theory Comput. 2013, *9*, 4046.
10. Ponder, J. W.; Richards, F. M., J. Comput. Chem. 1987, *8*, 1016.
11. Berendsen, H.J.C., J. Chem. Phys., 1984, 3684.
12. Anderson, H.C. J. Chem. Phys. 1980, 72, 2384.
13. Hoover, W.G. Physical Review A, 1985, 31, 1695.
14. Nosé, S. J. Chem. Phys. 1984, 81, 511.

15. Slater, J.C. Phys. Rev.1930, 36, 57.

16. Boys, S.F.; Proc. R. Soc. A. 1950, 200, 542.

17. Ditchfield, R.; Hehre, W.J.; Pople, J.A. J. Chem. Phys. 1974, 54, 724.

18. Koch, W. & Holthausen, M. C. A chemist's guide to density functional theory, 2008, Wiley-VCH.

19. Jensen, F. Introduction to computational chemistry 1999, Wiley.

20. Hohenberg, P. & Kohn, W., Phys. Rev. 1964, 136, B864.

21. Thomas, L. H., Math. Proc. Camb. Philos. Soc. 1927, 23, 542.

22. Lieb, E. H. & Simon, B. Adv. Math. 1977, 23, 22, 116.

23. Kohn, W. & Sham, L., J. Phys. Rev. 1965, 140, A1133.

24. Yanai, T., Tew, D. P. & Handy, N. C., Chem. Phys. Lett. 2004, 393, 51.

25. Cohen, A. J., Mori-Sánchez, P. & Yang, W., J. Chem. Phys. 2007, 126, 191109-1-5.

26. Tozer, D. J. & Handy, N. C., J. Chem. Phys. 1998, 108, 2545.

27. Boese, A. D. & Handy, N. C., J. Chem. Phys. 2002, 116, 9559.

28. Boese, A. D. & Martin, J. M. L., J. Chem. Phys. 2004, 121, 3405.

29. Cohen, A. J. & Handy, N. C., Chem. Phys. Lett. 2000, 316, 160.

30. Perdew, J. P. & Wang, Y., Phys. Rev. B 1992, 45, 13244.

31. Vosko, S. H., Wilk, L. & Nusair, M., Can. J. Phys. 1980, 58, 1200.

32. Cramer, C. J. Essentials of computational chemistry: theories and models, 2002, J. Wiley.

33. Kang, K., Science 2006, 311, 977.

34. Csonka, G. I., Éliás, K. & Csizmadia, I. G., Chem. Phys. Lett. 1996, 257, 49.

35. Huang, Y.-W. & Lee, S.-L., Chem. Phys. Lett. 2010, 492, 98.

36. Nolan, M., Grigoleit, S., Sayle, D. C., Parker, S. C. & Watson, G. W., Surf. Sci. 2005, 576, 217.

37. Jursic, B. S., J. Mol. Struct. 1997, 417, 89.

38. Bauzá, A., Alkorta, I., Frontera, A. & Elguero, J., J. Chem. Theory Comput. 2013, 9, 5201.

39. Becke, A. D., J. Chem. Phys. 1993, 98, 5648.

40. Lee, C., Yang, W. & Parr, R. G., Phys. Rev. B 2998, 37, 785.

41. Perdew, J. P.; Burke, K.; and Ernzerhof M.; Phys. Rev. Lett. 1996, 77, 3865.

42. Troullier, N.; Martins, J. L.; Phys. Rev. B 1993, 43, 1991.

Chapter 3 Results: Static Calculations and FPMD Simulations

3.1 Introduction – axial chirality

Biaryl molecules are broadly significant to fields such as pharmaceuticals, environmental protection, storage of toxic materials and small molecules, etc.[1-3] These applications depend on our ability to control the axial chirality of a biaryl molecule. This chapter aims to clearly outline and explain in depth the arguments for using a mechanochemical approach to achieving enantiomeric excess in axially chiral systems. Axial chirality describes the relationship of isoenergetic structures, called atropisomers, in systems that contain adjacent planes with staggered orientations.[4-8] Depending on the relative orientation of the two molecular planes, one of two atropisomers may exist with a planar TS separating them. Each atropisomer is a stable structure represented by a minimum on the PES. The conversion between atropisomers passing through the planar TS can be understood just as any reaction, by investigating reactant, product, and TS energies, and calculating reaction barriers.

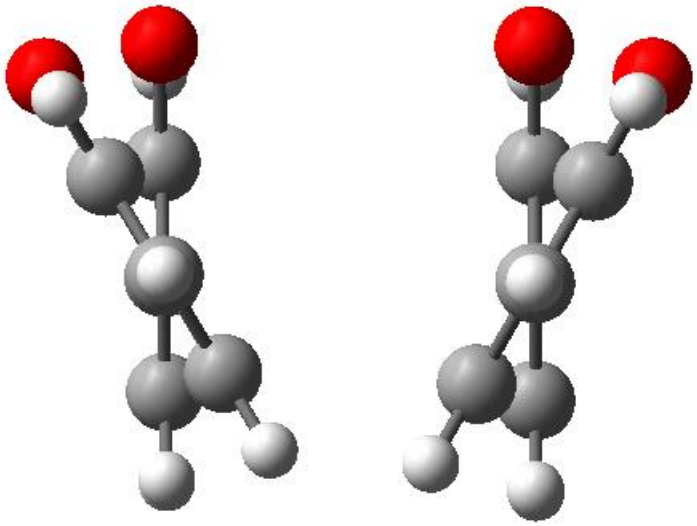

Figure 3-1. Atropisomer forms are presented using a generic representation of a substituted biaryl molecule. These atropisomers are enantiomers with respect to axial chirality. Axial chirality involves the relative orientation of adjacent planes in a molecule, as shown. Fine control of these atropisomers is of significant interest synthetically and pharmacologically.

In order to achieve enantiomeric excess in an axially chiral system, the isoenergetic nature of the atropisomers must be addressed. Mechanochemistry normally allows one to modify the PES along a reaction coordinate to lower barriers, and/or favor reaction products. An extension of this to achieve enantiomeric excess in axially chiral systems demands that mechanical force be used to distinguish between atropisomers. Tensile forces have difficulty accomplishing this due to the inherent symmetry of many axially chiral systems. For this reason, steps have been taken to incorporate τ into already existing mechanochemical methodologies. τ is capable of performing work over a torsional angle ϕ, thus introducing the needed energetic distinction between atropisomers based on the magnitude of τ and the angle ϕ. This is illustrated in figure 3.2. The work performed by F and τ on the PES is described by the following expression.

$$\boldsymbol{V(x, F, \tau) = V_{BO}(x) - Fq(x) - \tau\phi(x)} \qquad 3.1$$

where V(**x**,$\boldsymbol{F}$,$\boldsymbol{\tau}$) is the modified potential energy function, V_{BO} is the Born-Oppenheimer (unmodified) potential energy, x encompasses all nuclear coordinates, F is an external force performed over distance q(**x**), and τ is an external torque performed over a torsion ϕ(**x**).

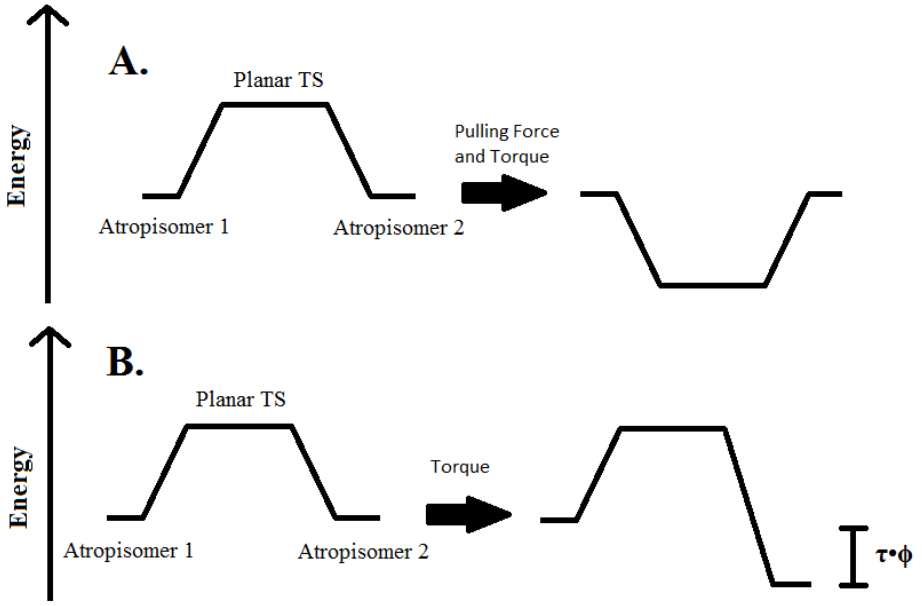

Figure 3-2: Illustrates how the rotational energy profile of an axially chiral system is influenced by F and τ. F and τ are both capable of lowering the planar TS energy. τ is unique in its ability to introduce an energetic deviation between atropisomers, which are normally energetically degenerate.

F cooperates with τ in this scheme. F lowers the rotational barrier between atropisomers by lowering the energy of the planar TS between them. If τ introduced an energetic distinction between atropisomers, but the planar TS precluded an inter-conversion between them, then no enantiomeric excess would be observed. F solves this problem by ensuring that the kinetics of rotation are such that each local minimum corresponding to an atropisomer can be sampled so that

thermodynamic equilibrium can be reached based on their energetic distinction. This provides a very simple basis for the approach. Throughout this work, o,o'-difluorobiphenyl was used as a general example of an axially chiral system. This biaryl system is illustrated in figure 3-3.

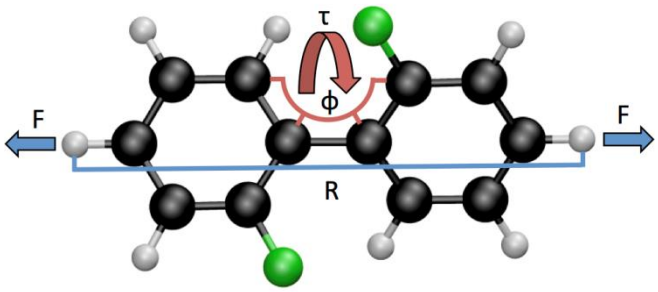

Figure 3-3: o,o'-difluorobiphenyl which was used as a simple model to represent axially chiral systems. Degrees of freedom R and ϕ are shown, to which F and τ were applied.

Careful consideration must be made to account for the relative energies of 4 key orientations of an axially chiral system. These orientations are illustrated in figure 3-4.

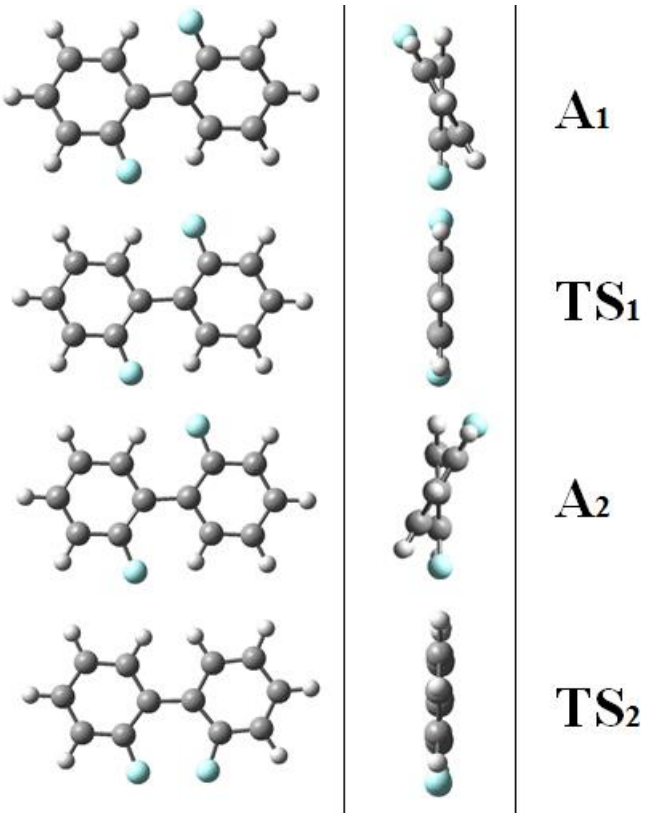

Figure 3-4: Key orientations of o,o'-difluorobiphenyl. A_1 and A_2 represent the two atropisomers. TS_1 and TS_2 represent the two planar transition states. These key orientations represent stationary points on a PES.

3.2 Introduction – classifying rotational behaviors

Three behaviors can be observed depending on the trends in these 4 energies: unchanged, locked, and freely rotating. The unchanged behavior is observed when insufficient F or τ have been applied. It is characterized by the distinct lack of changed behavior as compared to an unmodified system. Either the first TS is too high in energy for atropisomer conversion to occur, or there is insufficient energy difference between atropisomers. In either case, enantiomeric excess is not achieved. The second behavior, locked, occurs when an ideal combination of F and τ is applied such that enantiomeric excess is achieved. This occurs when sufficient τ has been applied

to thermodynamically select one atropisomer, and sufficient F has been applied to facilitate atropisomer conversion at a realistic timescale by lowering TS_1. Additionally, the energy of TS_2 is sufficiently high to prevent continued rotation through the selected atropisomer. High TS_2 ensures that the axially chiral system does not simply rotate continuously. The third behavior, freely rotating, is characterized by this continuous rotation. This occurs if too much F or τ has been applied to the extent that TS_2 is low enough for the system to pass through it at the same timescale as TS_1. This prevents the state populations from accumulating in favor of the second atropisomer.

3.3 Results - static energy calculations

It is clear that specific combinations of F and τ must be applied to achieve the locked behavior, and by extension enantiomeric excess. An interesting question is whether or not this range of acceptable F and τ combinations is suitably forgiving so as to make this process experimentally feasible. To address this question, static QC calculations were used in conjunction with geometry optimizations and frequency calculations in order to locate and characterize local minima on the FMPES. The torque contribution to the FMPES was incorporated into existing schemes as part of this work. Analytical and numerical frequency calculations were calculated in a τ dependent manner, and used for cross validation. The PBE XC functional and a 6-31G(d,p) basis set were used for these calculations.[9] Geometry optimizations were performed using NWChem.[10] All calculations were performed on a series of substituted biaryl compounds subject to F and τ in the range of 2000 pN and 200 pNÅ respectively. The purpose was to map out changes in rotational barriers as a function of F and τ. Characteristic results of these simulations are illustrated in figure 3-5.

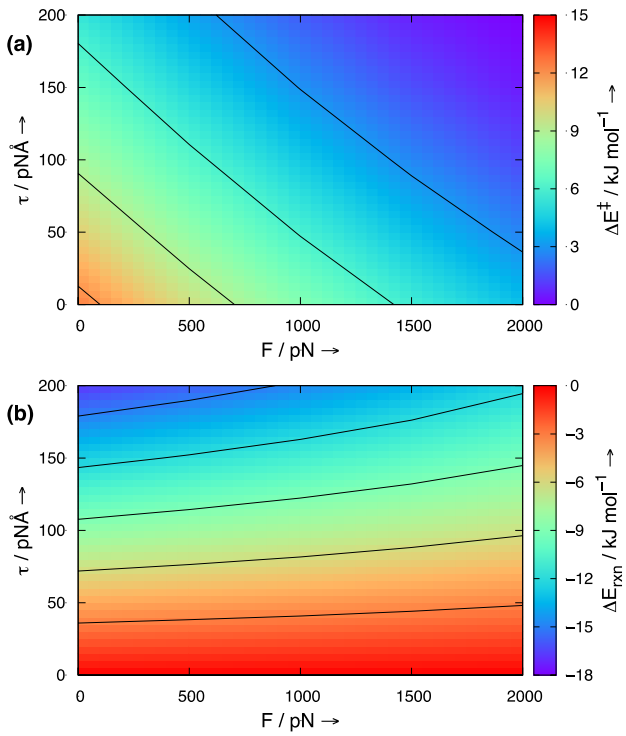

Figure 3-5: **a)** The relationship between the rotational barrier energy ($\Delta E^{\ddagger}$) for atropisomer inter conversion as a function of F and τ. The rotational energy barrier is presented in kJ/mol as obtained by static DFT calculations. Colored regions represent how F and τ work co-operatively to influence the rotational energetics of the biaryl system, bearing influence on the emergence of unchanged, locked, or freely rotating behaviors as previously described. **b)** The reactions energy (ΔE_{rxn}), the difference in energy between atropisomers as a function of F and τ. Values are presented in units of kJ/mol as obtained from static DFT calculations. It is clearly seen that F has no appreciable influence on the reaction energy. τ, however, introduces an energetic bias towards one atropisomer which may provide the basis for thermodynamic selection of said atropisomer within a broader mechanochemical scheme. When combined with the ability of F and τ to tune the rotational barrier energy, it is feasible to imagine that both the extent of atropisomer conversion, as well as the timescale of conversion, may be controlled with careful application of F and τ.

It is worth noting that the practical limitations which affect the upper limit on magnitudes of F and τ that can be realistically applied are not the same. F is limited by the fact that at high tensile forces, a molecular bond may be completely pulled apart and broken. This is the reason that these studies hesitate to go beyond a few thousand pN of tensile force. τ is less sensitive to this limitation because the force vector can be perpendicular to the bonds connecting the four torsional atoms over which it is applied. It appears that higher values of τ may be applied without physically ripping a molecule apart. This makes it an attractive option for mechanochemically controlling ΔE_{rxn}, and to a lesser extent $\Delta E^{\ddagger}$. Experimental work would prove the most valuable for exploring the upper limits of τ that could be applied.

Based on the results presented in figure 3-5, it is possible to imagine a mechanochemical scheme in which F and τ are used to lower the energy of atropisomer inter-conversion to an experimentally practical timescale, wherein τ can be leveraged to thermodynamically bias the system towards one atropisomer, producing enantiomeric excess. Although this is initially promising, more validation is required in order to support the idea that observable rotational behavior can be influenced by modifying the rotational energy profile. To this end, MD simulations were performed in order to observe how F and τ induced changes can influence rotational behavior.

3.4 Results - molecular dynamics simulations

A series of FPMD simulations were performed on o,o'-difluorobiphenyl shown in figure 3-3. MD simulations were performed using the Quantum-Espresso code suite with a time step of 6.0 a.u. and a planewave basis set with norm conserving pseudopotentials.[11,12] Simulations were performed at various combinations of F and τ within the limit of 2000 pN and 200 pNÅ

respectively. Central torsional angles were measured over the course of 5 ps simulations. Torsional data fell into one of three categories, illustrated in figure 3-6.

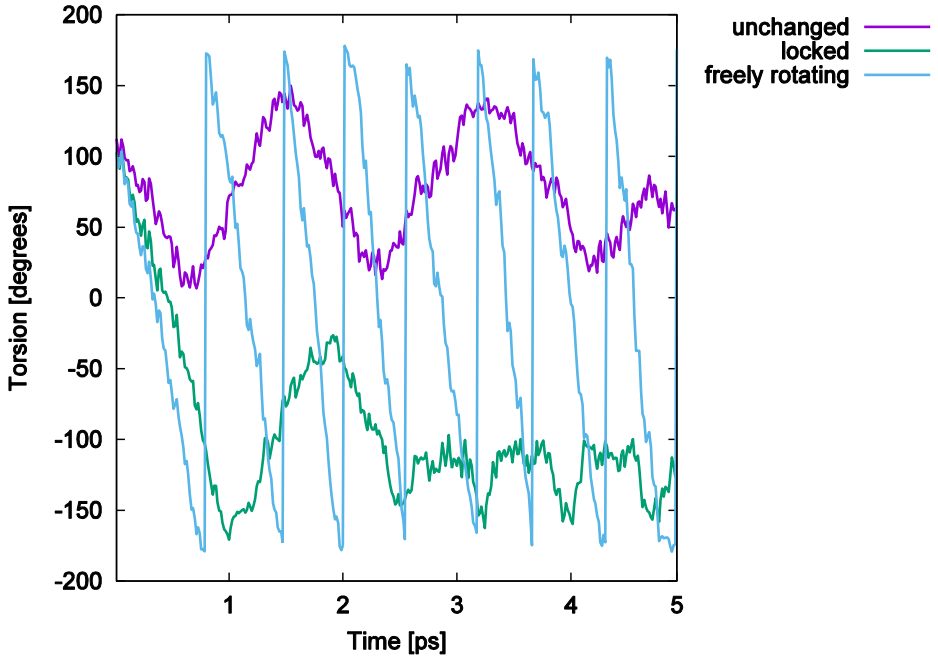

Figure 3-6: The torsional data collected over the course of a single 5 ps FPMD simulation will adhere to one three trends each corresponding to a rotational behavior. The unchanged behavior shows a torsion which only occupies a total range of 180 degrees. This biaryl is unable to pass through either TS_1 or TS_2 within a ps time scale. The locked behavior shows a torsion that initially exists in a range of 0 – 180 degrees, subsequently passing through TS_1 and becomes locked into the -180 – 0 degree range due to it's inability to pass through the higher energy TS_2. The freely rotating graph cycles through a full 360 degree torsion range because it easily passes through TS_1 and TS_2.

Torsional results were used to categorize each F and τ combination as producing unchanged, locked, or freely rotating behavior. The relationship between F. τ and rotational behavior has been mapped out in figure 3-7. FPMD behavioral mapping is coupled with a

rotational energy profile of the stationary states, A_1, TS_1, A_2, and TS_2, in order to reveal trends between the relative energies of the stationary states, and resulting rotational behavior.

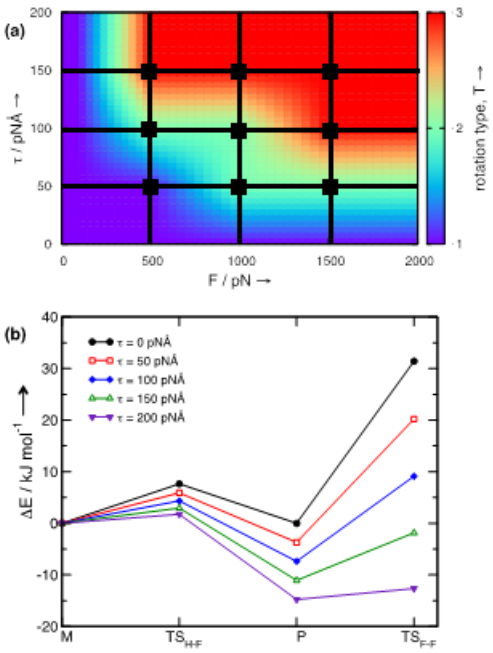

Figure 3-7: **a)** The mapping of rotational behavior onto a range of *F* and τ combinations. Torsional data from FPMD simulations was quantified based on how well it fit to one of the three trends illustrated in figure 3-6. Values of 1, 2 and 3 were assigned to behaviors of unchanged, locked, and freely rotating respectively. **b)** Energies of stationary points along reaction coordinate are presented to support the FPMD results. Points M, $TS_{H\text{-}F}$, P, and $TS_{F\text{-}F}$ are analogous to A_1, TS_1, A_2, and TS_2 respectively. Energetic trends over a rotational degree of freedom can be compared across a range of τ values, with a fixed *F* value of 1000 pN.

From the data presented in figure 3-7 it can be seen that rotational behavior progresses from unchanged to freely rotating in response to increases in *F* and τ. There is a band in the middle

where locked behavior occurs, corresponding to specific combinations of F and τ. This reflects a change in the rotational energy profile that allows transition through TS_1 from A_1 to A_2, whilst TS_2 remains large enough to prevent further rotation. This desirable energy profile for locked behavior can be easily understood by cross referring results in figures 3-7 a) and b). Figure 3-7 b) shows how the rotational energy profile changes with τ when F is fixed at 1000 pN. Figure 3-7 a) indicates that locked behavior is observed at τ = 100 pNÅ when F = 1000 pN. This is reflected well in figure 3-7 b) where the function corresponding to τ = 100 pNÅ shows that the energy of A_2 has been lowered relative to A_1 while TS_1 is also decreased; this combination would lead to an excess of A_2 forming. Additionally, the barrier formed between A_2 and TS_2 ($A_2 - TS_2$) is higher than that of $A_2 - TS_1$. Meaning that continued rotation from A_2 past TS_2 is unlikely, preventing the freely rotating behavior. These factors combined support the notion that locked behavior should be observed at F = 1000pN and τ = 100 pNÅ. In this sense, the FPMD results are consistent with previous prediction from static calculations. Values of τ above 100 pNÅ produce the freely rotating behavior in figure 3-7 a). This is once again supported by the results of figure 3-7 b). In the latter it can be seen that for values of τ above 100 Å the A_2-TS_2 barrier becomes smaller than the A_2-TS_1 barrier. This means that unless a substantial amount of energy was dissipated after the system relaxes from TS_1 to A_2, then there would be ample energy available to overcome the A_2-TS_2 barrier. The ease of passage through TS_2 is what produces the freely rotating behavior.

3.5 Robustness - level of theory, systems, pulling points

Static energy calculations were performed using a number of different basis sets and XC functionals. Results are presented in figure 3-8. The intention is to show that level of theory has no effect on how F and τ are able to perform work on the system. This is important to show that a

combined *F*. τ modified PES is not simply an artifact arising from a specific basis set and XC functional.

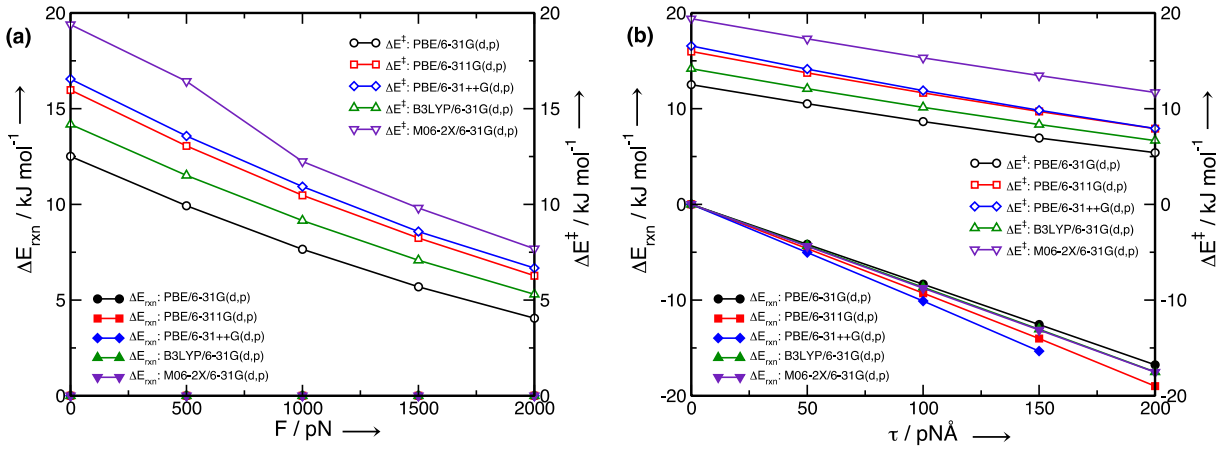

Figure 3-8: Reaction energies (ΔE_{rxn}) and rotational barriers ($\Delta E^{\ddagger}$) for o,o'-difluorobiphenyl subject to *F* and τ across multiple levels of theory. Results indicate that the effects *F* and τ are independent of the level of theory.

Due to practical computational limitations imposed by FPMD simulations, most of the results reported thus far were derived from o,o'-difluorobiphenyl. For practical applications of this method, however, the rotational barriers would likely be higher to prevent racemization at short timescales as would be seen in o,o'-difluorobiphenyl. The same approach taken with o,o'-difluorobiphenyl could be employed when dealing with a wide range of pharmaceutically relevant biaryl molecules. In order the demonstrate the robustness of this approach, three such biaryl systems with pharmaceutical relevance were subject to the same *F* and τ as o,o'-difluorobiphenyl. These systems are: (**2**: 2-biphenylcarboximidamide, **3**: 2,6-dimethylbiphenyl, **4**: 1-nitro,2-phenyltetrahydrofuran)**,** and are shown in figure 3-9. Rotational barriers, $\Delta E^{\ddagger}$, and reaction energies, ΔE_{rxn}, were calculated for each system.

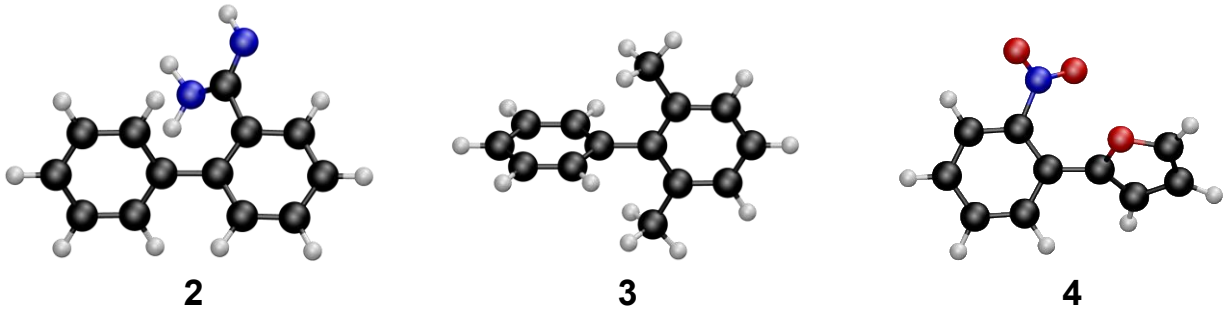

Figure 3-9: Structures of three pharmaceutically relevant biaryl molecules. All are characterized by the fact that their rotational barriers are higher than that of o,o'-difluorobiphenyl.

When figure 3-10 is compared to figure 3-5, it is clear that the general trends in $E^{\ddagger}$ and ΔE_{rxn} are maintained in systems with more hindered rotation. This is a predictable result, seeing as the mechanochemically induced change in energy across a torsion is simply related to the magnitude of τ and the range of ϕ over which it is applied. Both A_1 and A_2 have a ϕ deviation from TS_1 of between $\frac{1}{2}(\pi)$ and $\frac{1}{3}(\pi)$. Thus if the same range of τ is applied, the only expected results is that the energy change would be the same, because the change in ϕ involved to calculate ΔE_{rxn} and $E^{\ddagger}$ is predictable and relatively constant for biaryl molecules. This is an important idea which will be further developed in Chapter 4.

It is worthwhile to quickly reiterate the trends seen in both figure 3-10 and figure 3-5. $\Delta E^{\ddagger}$ represents the energy difference between A_1 and TS_1. It is clearly seen that $\Delta E^{\ddagger}$ shows a comparable response to both F and τ. This is expected as F is able to primarily lower the energy of TS_1 by relieving steric hindrance on its clashing ortho groups, whereas τ is able to provide work across the torsion ϕ separating TS_1 and A_1.

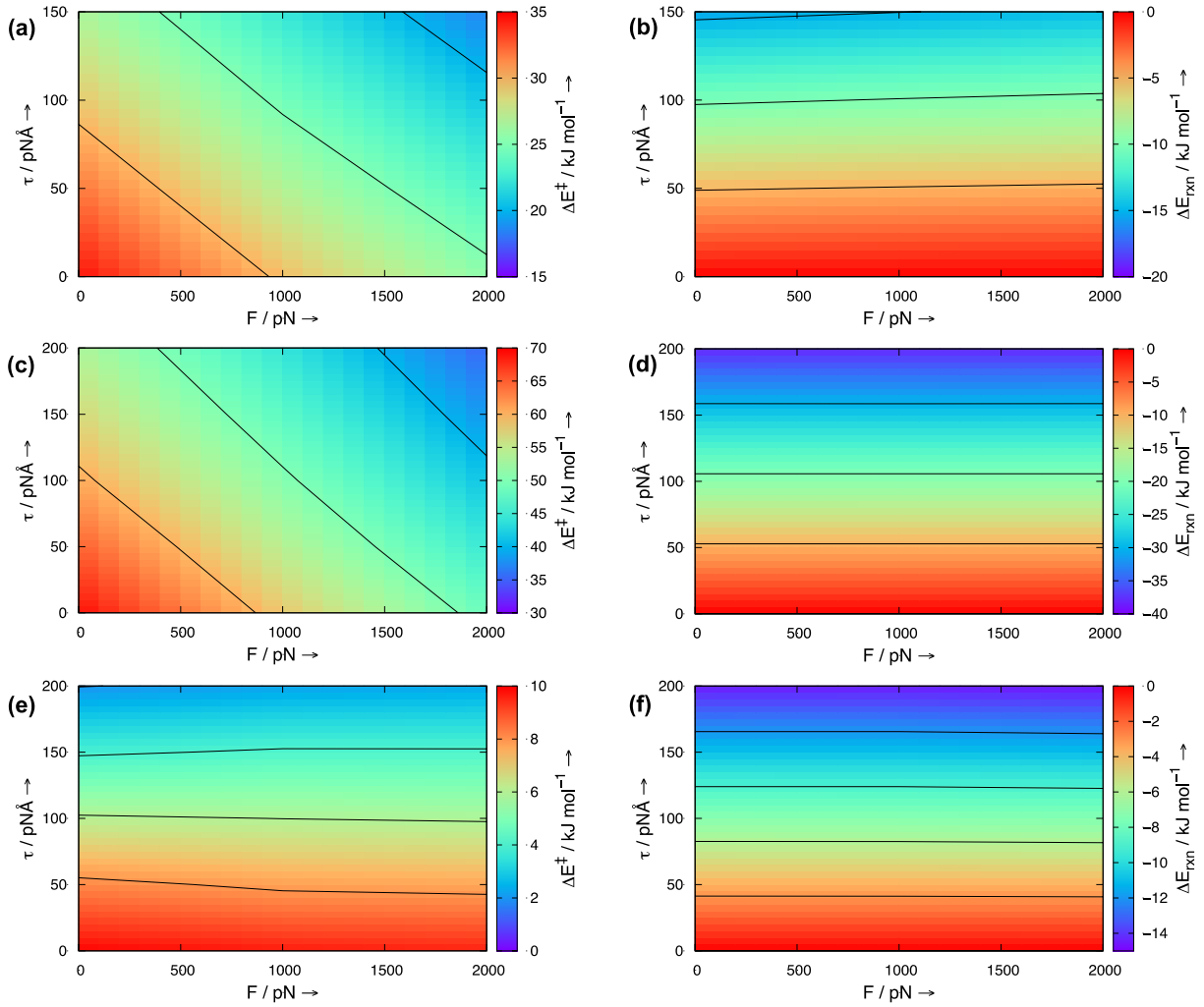

Figure 3-10: Rotational barriers and reaction energies for systems **2**, **3**, and **4** calculated at different values of F and τ. **(a)** $\Delta E^{\ddagger}$ for **2**. **(b)** ΔE_{rxn} for **2**. **(c)** $\Delta E^{\ddagger}$ for **3**. **(d)** ΔE_{rxn} for **3**. **(e)** $\Delta E^{\ddagger}$ for **4**. **(f)** ΔE_{rxn} for **4**.

The following aims to dispel the possible notion that the choice of pulling points is unforgiving. This is accomplished by calculating A_1, TS_1, and A_2 energies for o,o'-difluorobiphenyl subject to F applied to the ortho substituents. This is illustrated in figure 3-11.

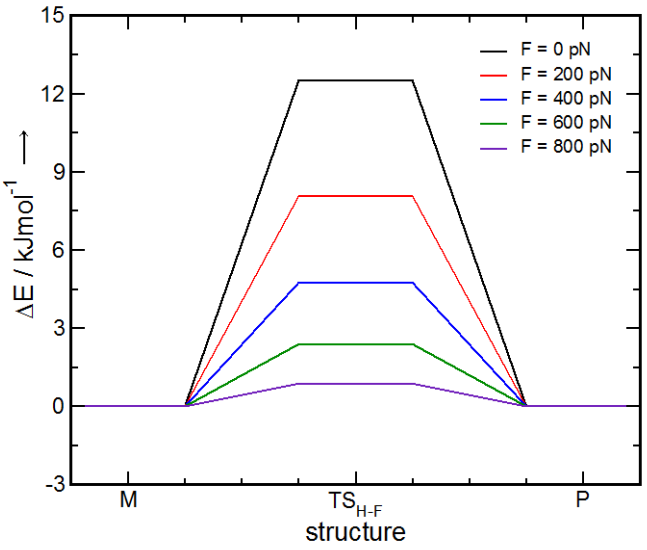

Figure 3-11: Change in energy that occurs as o,o'-difluorobiphenyl is converted from M to P through $TS_{H\text{-}F}$. M, P and $TS_{H\text{-}F}$ are analogous to A_1, A_2 and TS_1 respectively. *F* is applied to the fluorine atoms in the 2 and 2' positions of the biphenyl. The data shows that $\Delta E^{\ddagger}$ is reduced with increasing *F* but the atropisomers remain isoenergetic.

The results shown in figure 3-11 are consistent with the claim that acceptable variation exists in the choice of pulling points over which to apply *F*. In biaryl systems specifically, this is likely due to the large extent of force transmission made possible by the rigidity of the aromatic rings. It is reasonable to suggest that increasing the rigidity of a system would increase the robustness of results with respect to the choice of pulling points. In any case, the results obtained for ortho pulling points are in full agreement with those obtained for para pulling points, demonstrating at least some degree of robustness.

3.6 Discussion - manipulating rotational timescales

Recently published work has explored the time dependent nature of atropisomer inter-conversion in axially chiral pharmaceutical molecules.[2] In doing so, a connection has been made

between TS_1 and the timescale of atropisomer inter-conversion. This is illustrated in figure 3-12. It is also worth noting that the timescale of atropisomer rotation can also be heavily modulated by solvent effects.

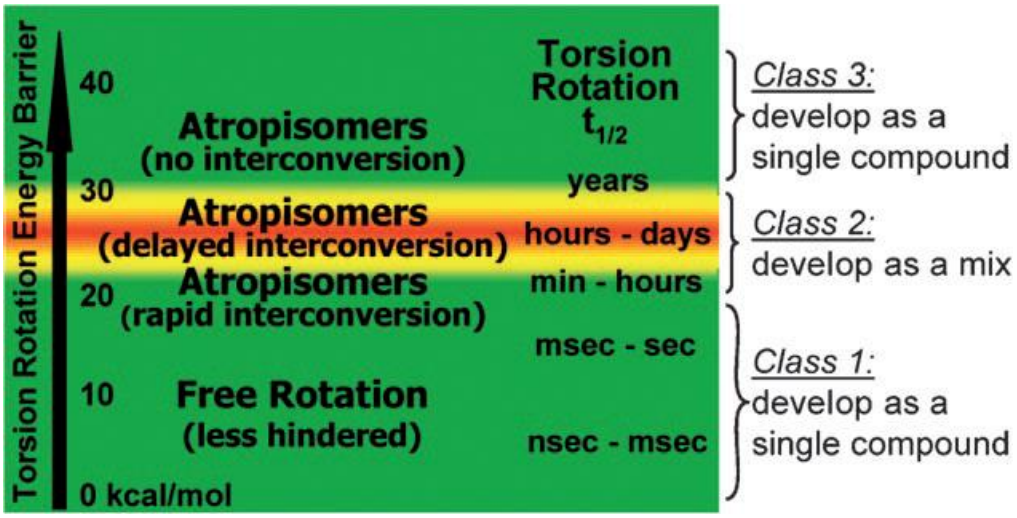

Figure 3-12: The relationship between the TS_1 barrier and the timescale of atropisomer inter-conversion.[2]

The FPMD simulations detailed previously show how locked behavior can be observed at picosecond timescales for o,o'-difluorobiphenyl. The data in figure 3-12 provide a map to illustrate the energy barrier targets needed to achieve locked behavior over a wide range of potential timescales. For instance, if locked behavior was desired at a minimum timescale of hours, then a rotational barrier may be mechanochemically lowered from some amount, down to 20-25 kcal/mol. This would ensure that atropisomer inter-conversion is accessible enough that a τ biasing effect could be felt, such that enantiomeric excess could be achieved.

The previous energy calculations and FPMD simulations used o,o'-difluorobiphenyl as a simple model system. Any extrapolation necessary for practical experimental relevance requires, however, a provably robust approach. For this purpose, a number of additional calculations have

been performed to demonstrate the robustness of this mechanochemical scheme to achieve enantiomeric excess. These address three areas: level of theory, structural variation of systems, and choice of pulling points.

3.7 Conclusions

The control of axial chirality is sought after for the broad usefulness of chirally pure biaryl molecules. Conventional mechanochemical approaches are ill suited to this task due to the fact that atropisomers are structurally symmetric with respect to the axis over which F is applied, and remain isoenergetic. τ is introduced due to the fact that it is rotationally anisotropic, and can be applied directly to the reaction coordinate which corresponds to a rotational degree of freedom (dof). τ can be used to control the reaction energy related to atropisomer conversion, while F is applied to lower the energy of the planar TS separating the atropisomers, enhancing the kinetics of conversion. Too much F and/or τ overshoots atropisomer selection and leads to continuous biaryl rotation. Conversely, careful application of F and τ promotes a single atropisomer, leading to enantiomeric excess. Dynamics simulations have shown that F and τ values can be selected quantitatively based on the results of static QC calculations across a range of F and τ values. Chapter 4 will continue to explore how ideal values of F and τ can be selected without the need for a large number of QC calculations.

References:

1. F. Leroux, ChemBioChem 2004, 5, 644.

2. S. R. LaPlante, ChemMedChem. 2011, 6, 505.

3. L. Ma, C. Abney, W. Lin, Chem. Soc. Rev., 2009, 38, 1248.

4. S.R. LaPlante, P.J. Edwards, L.D. Fader, A. Jakalian, O. Hucke, ChemMedChem 2011, 6, 505.

5. F. Leroux, ChemBioChem 2004, 5, 644.

6. L. Pu, Chem. Rev. 1998, 98, 2405.

7. R. Noyori, H. Takaya, Acc. Chem. Res. 1990, 23, 345.

8. M.W.A. MacLean et al., Chem. Mater. 2014, 26, 5852.

9. J. P. Perdew, K. Burke, and M. Ernzerhof, Phys. Rev. Lett. 1996, *77*, 3865.

10. M. Valiev, E.J. Bylaska, N. Govind, K. Kowalski, T.P. Straatsma, H.J.J. van Dam, D. Wang, J. Nieplocha, E. Apra, T.L. Windus, W.A. de Jong, Comput. Phys. Commun. 2010, *181*, 1477.

11. N. Troullier, J. L. Martins, Phys. Rev. *B* 1993, *43*, 1991.

12. P. Giannozzi et al., *J. Phys.* Condens. Matter. 2009, *21*, 395502.

Chapter 4 results: simplified model

Chapter 3 explored how specific combinations of F and τ enable atropisomer selection in o,o'-difluorobiphenyl. If experimental realization of mechanochemical enantioenrichment is the goal, then it is necessary to consider how an experimental lab might go about identifying the correct combination of F and τ required to achieve suitable enhancement of a desired atropisomer. The methods used in Chapter 3 involve static quantum chemical calculations and dynamics simulations (detailed in Chapter 2) and as such may be too cumbersome or time consuming for general use. To this point, a simplified model for low-cost optimization of F and τ for experimental enantioenrichment is likely necessary. This chapter explores the details of just such a proposed model.

4.1 Outline of General Approach

Similar to Chapter 3, a simple o,o'-dimethylbiphenyl system will be used in this chapter to illustrate the model being proposed. This allows for easy comparison between the results obtained from the simplified model, and those obtained from the more demanding methods employed in Chapter 3. It also provides a model system to easily illustrate the concepts underlying the many approximations that will be made by the model.

Just as before, o,o'-dimethylbiphenyl will be described by an inner torsion, ϕ, over which τ is applied, and pulling point distance R, over which F is applied. These are illustrated once again in Figure 4-1. Like before, particular focus will be drawn upon the stationary states along the reaction coordinate connecting the two atropisomers. Previously, these were defined as A_1, TS_1, A_2, and TS_2. Within this simplified model however, certain steps require restrictions to be placed on these structures. More specifically, fixed ϕ values will be assigned to each of these structures,

as illustrated in Figure 4-2. The minimum energy structures, 1_a and 3_a, have ϕ fixed to -π/2 and π/2 respectively, while TS structures $2^{\ddagger}$ and $4^{\ddagger}$ have ϕ fixed to 0. These fixed angles are imposed in order simplify the mathematical solutions required in order to optimize F and τ, which will be shown in detail later in this chapter. These fixed ϕ values are a fair assumption when considering the nature of almost all experimentally relevant biaryl molecules to which this approach may be applied. Biaryl molecules with rotational barriers above ~20 kJ/mol (most fall into this category) are sterically encumbered to the extent that they experience considerable repulsive forces even at ϕ values of 30 or 40 degrees. This hindrance pushes their minima structures even farther away from the planar structure towards ϕ values much closer to 90 degrees. Incidentally o,o'-difluorobiphenyl is one of the few biaryl molecules that does not have a 90 degree torsion, making it a suitable test system for this model seeing as it will demonstrate an upper limit on the error that this fixed torsion assumption may introduce.

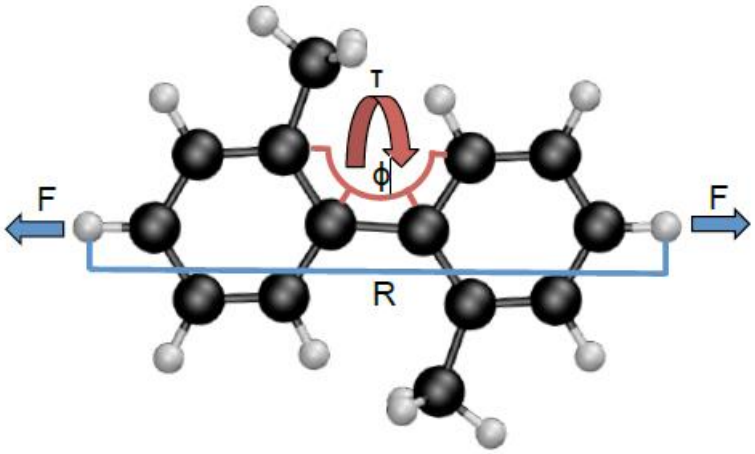

Figure 4-1: o,o'-dimethylbiphenyl which was used as a simple model to represent axially chiral systems. Degrees of freedom R and ϕ are shown, to which F and τ were applied.

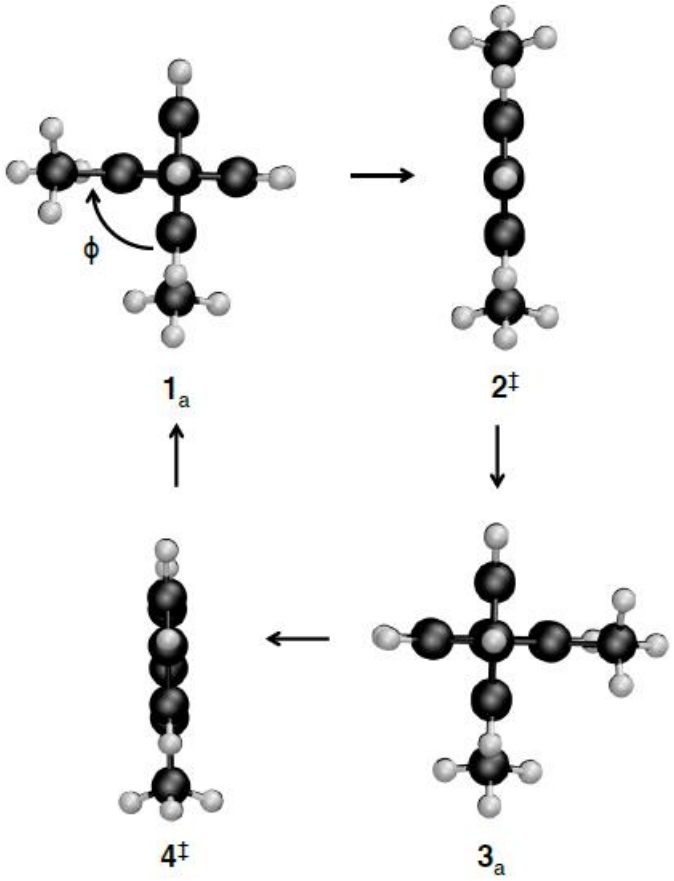

Figure 4-2: The four states that will be of most importance in the simplified model detailed in this chapter, as well as their corresponding fixed torsions. Approximate minimum energy structures 1_a and 3_a have ϕ Fixed to $-\pi/2$ and $\pi/2$ respectively, while TS structures $2^{\ddagger}$ and $4^{\ddagger}$ have ϕ Fixed to 0. These states correspond to A_1, A_2, TS_1, and TS_2 respectively, from chapter 3. The names have been changed to reflect the fixed torsion assumption. These fixed torsions are only used for the steps which directly calculated the optimized F and τ values.

The impact of F and τ along the reaction coordinate corresponding to rotation between atropisomers can be easily visualized. First, it is important to get a rough idea of what the unmodified reaction coordinate looks like; a sketch of this is shown in figure 4-3. In order to

achieve enantiomeric excess there are a few energetic requirements that must be met along the reaction coordinate:

(1) The energy of 3_a must be lowered relative to 1_a. Therefor the difference in energy between 3_a and 1_a must be negative ($\Delta_{31}<0$) This can be accomplished only through τ.

(2) The energy of $4^{\ddagger}$ must remain higher than $2^{\ddagger}$, otherwise free rotation will occur. Therefore the difference in energy between $4^{\ddagger}$ and $2^{\ddagger}$ must be positive ($\Delta_{42}>0$). τ lowers Δ_{42}, thus this requirement places an upper limit on the magnitude of τ that can be applied. The effect of F on Δ_{42} is minimal, and the assumption is made that it is insignificant.

(3) The barrier between 1_a and $2^{\ddagger}$ (Δ_{21}) must be low enough for rotation at a timescale that fits experimental convenience. F lowers the energy of $2^{\ddagger}$ and $4^{\ddagger}$ uniformly, without influencing Δ_{31} or Δ_{42}. Thus, F can be reserved as a parameter to control the timescale of rotation.

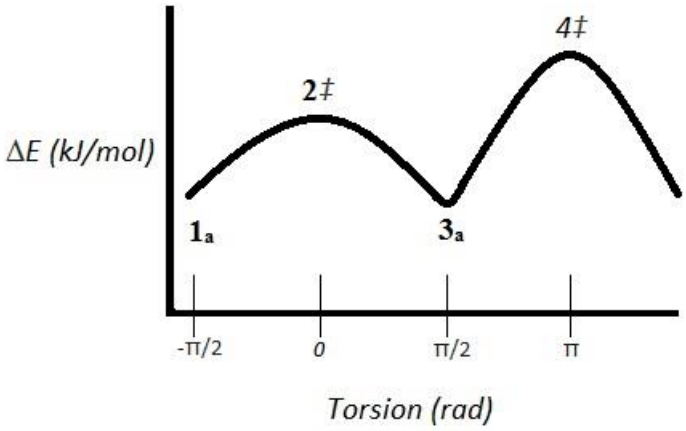

Figure 4-3: A rough sketch of the energy profile of a biaryl molecule along the reaction coordinate corresponding to atropisomer conversion. This will serve as a template with which to visualize the changes imposed by F and τ in order to achieve enantiomeric excess.

At this point, a vision of a procedural outline starts to form, wherein a maximum value of τ is applied to lower Δ_{31}, under the condition that Δ_{42} remains positive, otherwise free rotation would occur. At this point, the thermodynamic driving force for selection of 3_a has been established. Then, F is applied to lower Δ_{21} to some pre-defined level set for experimental convenience. This series of conditional statements lends itself well to an automated procedure, however it is still reliant on the ability to calculate a FMPES that responds to F and τ. As previously mentioned, the methods employed in Chapter 3 are too cumbersome, so a simplified approach must be devised for approximating a FMPES to which the above procedure can be applied. Section 4.2 outlines the steps and limitations involved in generating an approximated FMPES along the reaction coordinate (for atropisomer conversion) of a generic substituted biaryl.

4.2 Approximating the (F, τ)-modified PES

First, a quick review of the expression for a F and τ sensitive FMPES:

$$E(\boldsymbol{x}, \boldsymbol{F}, \boldsymbol{\tau}) = E_{BO}(\boldsymbol{x}) - FR - \tau\phi \tag{4.1}$$

where E_{BO} is the force un-modified Born-Oppenheimer (BO) PES, $\boldsymbol{x}$ represents 3N - 6 internal degrees of freedom, R is the pulling point distance over which F is applied, and ϕ is the torsional angle of central biaryl rotation over which τ is applied. As discussed in chapter 2, this equation provides the means to operate on a F and τ modified PES while still remaining analytically differentiable, thus allowing for geometry optimizations/characterization and frequency calculations. The only assumptions made here of relevance to experimental work are that F and τ can be evenly applied along specific degrees of freedom (R and ϕ).

The first step towards approximation involves considering the structural perturbations imposed by F and τ:

$$E(x, F, \tau) = E_{BO}(x^0) + \delta E_{BO}(\delta x) - F(R^0 + \delta R) - \tau(\phi^0 + \delta\phi) \tag{4.2}$$

where R^0, ϕ^0 represent values of R and ϕ before F, τ perturbation, and δR, $\delta\phi$ represent the magnitude of said changes in R and ϕ as a result of the perturbation. $\delta E_{BO}(\delta x)$ can be approximated by employing a second-order Taylor series approximation at x^0 on the BO PES. Fortunately, the first order term is necessarily zero, because x^0 corresponds to a stationary point structure. This leaves:

$$\delta E_{BO}(\delta x) = \frac{1}{2}\delta x^T H \delta x \tag{4.3}$$

where H is the Hessian matrix which includes degrees of freedom R and ϕ. F and τ effects can be communicated through the application of a stress vector, σ, which is composed of all zero elements, save for those along the R and ϕ degrees of freedom, with corresponding magnitudes F and τ accordingly. δx can be expressed in terms of σ as follows:

$$\delta x = H^{-1}\sigma = C\sigma \tag{4.4}$$

where C is the compliance matrix, which is the inverse of the Hessian. Substituting this into Eq. 4.3 yields:

$$\begin{aligned} \delta E_{BO}(\delta x) &= \frac{1}{2}\sigma^T C \sigma \\ &= \frac{1}{2}\left[C^{RR}F^2 + 2C^{R\phi}F\tau + C^{\phi\phi}\tau^2\right] \end{aligned} \tag{4.5}$$

where C^{RR}, $C^{R\phi}$, and $C^{\phi\phi}$ correspond to components of C that reflect to degrees of freedom R and ϕ in varying combinations. Expressions for changes in R and ϕ can similarly be obtained:

$$\delta R = C^{RR}F + C^{R\phi}\tau$$

$$\delta\phi = C^{R\phi}F + C^{\phi\phi}\tau \tag{4.6}$$

Eqs. 4.5 and 4.6 can be inserted into Eq. 4.2 to obtain:

$$E(x, F, \tau) \approx E_{BO}(x^0) - FR^0 - \tau\phi^0 - \frac{1}{2}\left[C^{RR}F^2 + 2C^{R\phi}F\tau + C^{\phi\phi}\tau^2\right] \tag{4.7}$$

This approximation can be used to extrapolate any stationary point on a BO PES to that of a (F,τ)-modified PES. This allows for FMPES energies to be calculated for minima and TSs so that reaction barriers, energies, and other useful parameters such as Δ_{42}, Δ_{31}, or Δ_{21} (ie. Relative energies) may be calculated in a time efficient manner.

Relative energies can be approximated according to the following scheme based off of Eq. 4.7:

$$\Delta E_{ij}(F, \tau) = \Delta E_{ij}^0 - F\Delta R_{ij}^0 - \tau\phi_{ij}^0 - \frac{1}{2}\left[\Delta C_{ij}^{RR}F^2 + 2\Delta C_{ij}^{R\phi}F\tau + \Delta C_{ij}^{\phi\phi}\tau^2\right] \tag{4.8}$$

where ΔE_{ij}^0 is the relative energy between stationary points denoted i and j on an unmodified PES, ΔR_{ij}^0 and ϕ_{ij}^0 are the un-(F,τ)-modified differences in R and ϕ between structures i and j, and ΔC_{ij}^{RR}, $\Delta C_{ij}^{R\phi}$, and $\Delta C_{ij}^{\phi\phi}$, are the changes in compliance matrix elements between structures i and j on an unmodified PES along combinations of the R and/or ϕ degrees of freedom. The first three terms are sufficient to approximate a system that is not subject to *F* or τ, the final term is responsible for incorporating the effects of structural changes imposed by said forces. It is important to re-iterate

that the compliance matrix elements used here are derived from the force-unmodified structure. Practically speaking, these would be provided by the results of a single QC calculation on a force unmodified structure. Critically, the ϕ limitations imposed and illustrated in figure 4.2 do not apply to these compliance matrix elements. Torsional limitations only apply to the subsequent steps which directly optimize F and τ. In other words, the torsional limitations only directly apply to $\delta\phi$ in equation 4.2.

4.3 Validation of Approximated Relative Energies

In order to validate the accuracy of the simplified model for approximating relative energies, comparison have been made between various relative energies calculated through QC calculations as seen in chapter 3, against those calculated using the simplified model (Eq. 4.8). The PBE XC functional and a 6-31G(d,p) basis set were used for these calculations.[1] Geometry optimizations were performed using NWChem.[2] The parameters obtained by QC calculations correspond to a geometry optimized force unmodified structure. This optimized structure is not subject to torsional restraints, and as such the properties derived from it are unaffected by it. The parameters calculated for o,o'-dimethylbiphenyl are shown in table 4-1.

Table 4-1. Pulling point distances, torsions, and compliance matrix elements for o,o'-dimethylbiphenyl Obtained from QC calculations.

R^0 [Å]	9.284	9.449	9.284	9.378
ϕ^0 [º]	91.1	180.0	268.9	353.5
C^{RR} [Å/pN]	21.164	19.132	21.164	8.456
$C^{R\phi}$ [º/pN]	-0.669	0.002	0.669	3.635
$C^{\phi\phi}$ [º/pNÅ]	130.949	5.267	130.949	603.456

Comparison of the reaction energy calculated via QC calculations or equation 4.8 is shown in Figure 4-4 a). Any disagreement between the two calculations appears to be mostly insensitive to F, whereas τ appears to have some correlation to the disagreement. At the maximum magnitude of τ tested, the disagreement in reaction energy reaches a peak of ~3 kJ/mol. This is likely due to the fact that τ has a significant influence on the stable structures of A_1 and A_2, as is reflected in the high magnitude of their compliance matrix elements along the ϕ dof ($C^{\phi\phi}$) values which are both 130.949 ^{0}/pNÅ. The approximate method uses a truncated Taylor series to estimate the energetic effects of these structural perturbations, however these approximations become poorer the greater the magnitude of the perturbation. Therefore in cases where the structural changes are large, the approximation will show appreciable error.

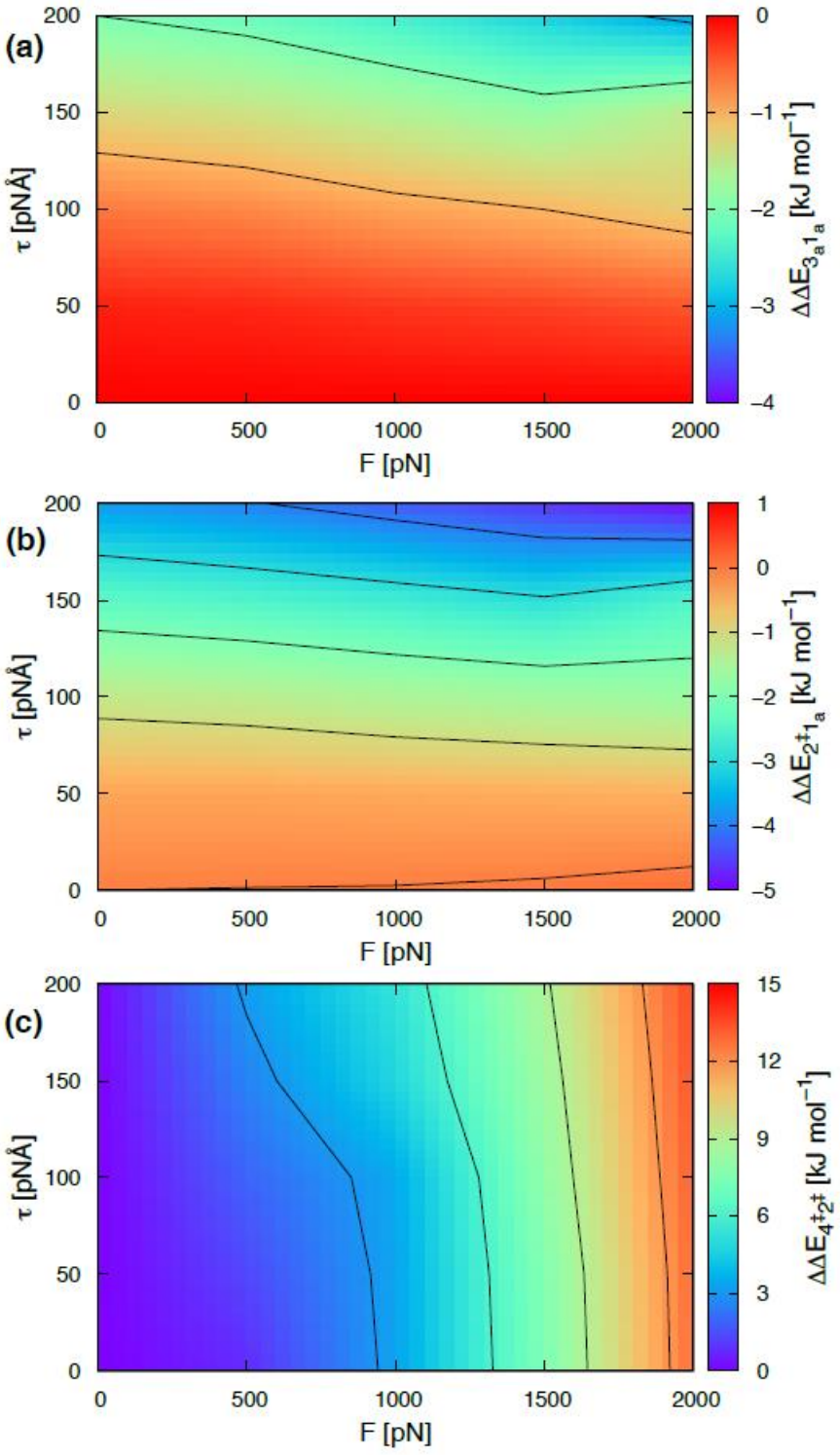
(a)
τ [pNÅ]
F [pN]
$\Delta\Delta E_{3a^1a}$ [kJ mol^{-1}]
(b)
τ [pNÅ]
F [pN]
$\Delta\Delta E_{2^\ddagger 1_a}$ [kJ mol^{-1}]
(c)
τ [pNÅ]
F [pN]
$\Delta\Delta E_{4^\ddagger 2^\ddagger}$ [kJ mol^{-1}]

Figure 4-4. Above illustrates the difference in **a)** reaction energies (Δ_{31}), **b)** reaction barriers (Δ_{21}), and **c)** relative TS energies (Δ_{42}) as calculated using QC calculations from chapter 3, or the approximation method based on the simplified model and equation 4.8. General agreement can be observed between the two methods within the range of a few kJ/mol.

Comparison of reaction barriers Δ_{21} are shown in figure 4-4 b). As before, the error is insensitive to *F*, and slightly sensitive to τ. The magnitude of error displayed is higher than that observed for the reaction energy, reaching a peak of ~5kJ/mol. This is likely due to the difference in how structures A_1 and TS_1 respond to τ. As previously mentioned, τ has a large effect on the structure of A_1, perturbing it towards a more planar structure. Structure TS_1, however, is largely insensitive to τ. This is reflected in their $C^{\phi\phi}$ values which are 130.949 ^{0}/pNÅ and 5.267 ^{0}/pNÅ respectively. In the case of the reaction energy, both A_1 and A_2 responded to τ nearly equally. Because the reaction energy is calculated as the difference in the energy values of these two structures, the errors in each nearly cancel out when their difference is taken, causing the overall error in reaction energy to be small. In the case of reaction barriers, however, the error in the energy of A_1 subject to τ is dissimilar to that of TS_1 subject to τ, therefore they do not cancel out, increasing the overall error in the calculated reaction energy. *F* demonstrates little impact on the error because it only makes minor, and similar, changes to the structures of A_1, TS_1, and A_2.

Comparison of TS_1 and TS_2 energies are shown in figure 4-4 c). Once again, the magnitude of the error has increased, reaching a peak of ~15 kJ/mol. This is a unique case, however, as *F* induced changes are far more significant in their contribution to the discrepancy between the QC calculations and the approximate method. This is, once again, due to force induced structural changes. TS_1 in its unperturbed state is effectively fully planar due to the lack of steric

hindrance of its ortho groups. TS_2 however, is skewed from a planar structure by ~7^0 due to the high amount of steric hindrance from clashing ortho methyl groups. *F* is a force that makes a structure more planar; TS_1 is already planar to begin with and therefore experiences little change, whereas TS_2 is skewed by several degrees and moves closer to a fully planar structure as the magnitude of *F* the applied increases. This is because *F* applied along R alleviates the steric hindrance of the clashing ortho groups and allows π stacking interactions to dominate, pulling the system towards a more planar structure. In other words, higher *F* values cause increasing levels of perturbation in the structure of TS_2, which leads to a poorer Taylor series approximation of the energy of TS_2 under the proposed approximate model. It is worth noting that the error introduced by *F* does not become appreciable until magnitudes higher than ~500 pN. This is because $F \leq 500$ pN are not sufficient to appreciably change the structure of TS_2.

An overall assessment of error shows that most calculations, such as reaction energy and barrier energy, maintain an acceptable error under 5 kJ/mol. However, the Δ_{42} calculation shows a markedly higher error with respect to F, reaching as much as 15 kJ/mol for the dimethylated system. This is particularly important upon review of the external force optimization process outlined in section 4.1. The process for optimizing τ involves lowering the Δ_{42} energy to a minimum allowed value set based on acceptable parameters for experimental atropisomer conversion. In other words, lower Δ_{42} as much as possible, but not so much that free rotation occurs and a desired atropisomer can no longer be isolated. Unfortunately, the parameter most susceptible to error is the Δ_{42} energy. This makes the critical process of optimizing τ prone to significant error. This is an important point which will be revisited in section 4.4.

4.4 Future Work – finalizing F and τ optimization procedure

The general process for optimizing the magnitude of F and τ required to achieve atropisomer selection must be implemented into a procedure following equation 4.2, using input approximated with equation 4.8. A simple example of such a procedure follows, first for τ:

$$\Delta_{42} = \Delta_{42}^{o} - \tau\pi$$
$$\tau = (\Delta_{42}^{o} - \Delta_{42})/\pi \tag{4.9}$$

where τ is the optimized value of torque applied in order to achieve excess of one atropisomer, Δ_{42}^{o} is the energetic difference of the two planar TS structures TS_1 and TS_2 with no external forces applied, Δ_{42} is the difference in TS energies after forces have been applied, and π is the approximate angle over which τ is applied between structures TS_1 and TS_2 due to torsional restrictions illustrated in figure 4-2. It has been assumed for this simple example procedure that the difference in $C^{\phi\phi}$ values for structures 4 and 2 is zero. The procedure is continued to optimize F:

$$d = \Delta_{21}^{0} - \Delta_{21}$$
$$d = F^2(\Delta C_{21}^{RR}) + F\left(\Delta R_{21}^{o} + \Delta C_{21}^{R\phi}\tau\right) + F^0(\Delta C_{21}^{\phi\phi}\tau^2 + \tau\frac{\pi}{2})$$
$$0 = F^2(a) + F(b) + F^0(c - d) \tag{4.10}$$

where a, b, and c are the bracketed terms in the second line, d is the difference in Δ_{21} energy barriers between the force modified (Δ_{21}) and un-force modified (Δ_{21}^{o}) structures. d is chosen based on the desired rate of atropisomer interconversion through TS_1, related to favored experimental kinetics. ΔR_{21}^{o} is the change in pulling point distance over which F is applied between structures TS_1 and

A_1, and ΔC values are compliance matrix elements along the R and ϕ dof which correspond to F and τ respectively. The process of optimizing F continues as the quadratic function is solved:

$$F = \frac{-b+\sqrt{(b^2-4a(c-d))}}{2a} \tag{4.11}$$

The root of the quadratic equation yields an optimized value of F, which is dependent on the previously optimized value of τ, as well as the input variable d.

It is worth quickly outlining the assumptions and limitations of this approach. First, by handling the τ optimization separately, and first, there is an assumption made that the Δ_{42} barrier is only modified by τ. This is of course not true, as F can slightly modify the Δ_{42} barrier. As a result, the τ value produced following this procedure should be an over-estimate. By not including compliance matrix element terms in the expression for τ we are also assuming that the TS_1 and TS_2 structures are not changing in response to τ. This is a good assumption as it has been shown through QC calculations that the structures of TS_1 and TS_2 are very rigid, and relatively insensitive to τ. It has also been assumed that the angle of separation between TS_1 and TS_2 is exactly π radians, and the separation between TS_1 and A_1 is $\pi/2$ radians. For almost all experimentally relevant systems, this is a good assumption. The final assumption is simply a reiteration of the inherent approximation involved in expanding upon a force-unmodified structure using a truncated second-order Taylor series, as described in section 4.2.

A procedure like the one above could be easily executed with short scripts, however there are a number of severe limitations that prevent the results from being useful at this stage. The limited capacity with which Δ_{42}, Δ_{21}, Δ_{31} values can be approximated have been outlined in section 4.3. These factors may contribute to discrepancies between the predicted and expected values for

both F and τ. More importantly, the procedure has been designed as a simple way of illustrating what a F and τ optimization process may look like. For this reason, it makes a large number of assumptions. One of the most egregious is to assume that F is zero during the τ optimization step. This was done to eliminate cross terms and make the procedure more simple, however the cooperation of F and τ is at the heart of this work, and so a final procedure should include F and τ cross terms. Additionally, there is no need to focus on the difference in Δ_{42} energies when optimizing τ, or Δ_{21} energies when optimizing F. There are a number of different approaches that could be taken for these optimization steps, such as using changes in barrier energies rather than relative TS energies for optimizing τ. There is a great flexibility in possible procedures; however some will require more assumptions than others. The example procedure provided in this section is not the most accurate, but rather is very clean and simple. It has been designed to illustrate an idea, rather than to be accurate for practical application. Future work must involve designing a procedure for optimizing F and τ which utilizes parameters calculated on a force unmodified structure, while making as few, or as sensible, further assumptions as possible.

References:

1. J. P. Perdew, K. Burke, and M. Ernzerhof, *Phys. Rev. Lett.* 1996, *77*, 3865.
2. M. Valiev, E.J. Bylaska, N. Govind, K. Kowalski, T.P. Straatsma, H.J.J. van Dam, D. Wang, J. Nieplocha, E. Apra, T.L. Windus, W.A. de Jong, *Comput. Phys. Commun.* 2010, *181*, 1477.

Chapter 5: conclusions and future work

Axial chirality is an interesting molecular property with relevance to a wide breadth of important systems.[1-3] Axial chirality in biaryl derivatives touches on a number of fast growing fields and applications: MOFs, liquid crystals, pharmaceuticals, environmental protection, small molecule storage etc.[4-8] Pursuit of much sought after chiral purity within a large variety of substituted biaryl molecules is currently a difficult and cumbersome process, requiring that unique synthetic procedures be designed for each and every biaryl system. This is particularly problematic for applications such as MOFs which ideally require large numbers of unique substituted biaryls to be synthesized in a chirally pure fashion. Mechanochemistry has to potential to provide a robust method of providing enantiomeric excess of axial chirality, and is an approach that applies nearly ubiquitously to a large number of substituted biaryl molecules, without the need of entirely separate procedures on a system-by-system basis.

Results presented in chapter 3 of this thesis have demonstrated how biaryl systems exhibit predictable rotational behaviors than can be associated with the relative energy levels of key stationary points along the rotational degree of freedom across the central torsion of the molecule. Furthermore, one of these behaviors (locked behavior) leads the system directly towards enantiomeric excess. By extension, if the relative energy levels of key stationary points along the rotational dof can be manipulated such that they tend towards the desired rotational behavior linked with enantiomeric excess, then a procedure can be envisioned in which manipulation of key structural energies leads to enantiomeric excess. Proper manipulation of these structural energies requires both F and τ. F alone is insufficient because it has no means of distinguishing between atropisomers, which are symmetric with respect to the rotational dof. τ introduces a necessary

anisotropy to the rotational dof which provides the basis for the energetic divergence of the atropisomers. Specific combinations of F and τ can be used to provide relative structural energy levels that are in line with the desired rotational behavior. QC calculations have been extended to provide work contributions of F and τ to the BO PES to allow for the identification of F and τ values required to achieve the desired relative energy levels.

The identification of F and τ values required to achieve enantiomeric excess require a large number of QC calculations at varying amounts of F and τ. The burden of this process can be lessened by instead approximating the effects of F and τ on the BO PES through employment of a truncated second order Taylor series approximation centered on the force-unmodified structure. This way, a single QC calculation is performed on an unmodified system. Parameters obtained from this system such as compliance matrix elements are used to approximate the effects that F and τ would have based on the degree of structural change that they would induce. The result is a more time efficient manner in which the F and τ effects on the relative energies of key structures along the rotational dof can be calculated, such that a set of relative energies corresponding to enantiomeric excess can be associated with an ideal F and τ combination. This forms the basis for a practical procedure used to find F and τ values that will produce enantiomeric excess; chapter 4 has outlined this procedure in precise detail, along with outstanding limitations and setbacks.

The use of mechanochemistry to achieve enantiomeric excess in axially chiral systems is burdened by a number of practical limitations. Currently, the ability to perform mechanochemical work on single molecules in a precise way along specific degrees of freedom is difficult to achieve at an industrial scale. For purposes such as pharmaceutical manufacturing, mechanochemistry is not practical for producing large quantities of chirally pure product, and unique asymmetric

synthesis strategies are still required. It is possible that advances in mechanochemical methods, such as magnetic torque tweezers (MTT), could allow for up scaling of force application to an industrial scale, however a lot of progress still needs to be made in this and other experimental mechanochemistry techniques. In the meantime, applications such as MOF synthesis provide an interesting platform for the utility of sub-industrial quantities of chirally pure biaryl systems. MOF synthesis requires a small amount of BINAP based axially chiral linker ligands, which normally require asymmetric synthesis strategies, but could greatly benefit from a broadly applicable mechanochemical approach. The small quantity of linker ligand needed sidesteps the low throughput of a mechanochemical enantioenrichment procedure.

An interesting avenue for future research may focus on how F and τ propagate their effects throughout a system's many dofs, originating from their initial PPs, as well as how quantifiable descriptors may be related to this propagation. This would allow for mechanochemical approaches involving F and τ to be extended to systems outside of substituted biaryls. For instance, it is known that certain properties within a biaryl allow for the application of F at the para positions, which is perpendicular to the central torsional dof, to indirectly influence rotation. These properties include π stacking interactions and the stiffness of aromatic systems. The π stacking interactions stabilize the planar TS, and these interactions become more dominant as F applied at the para positions relieves ortho steric hindrance. In this way, as F increases, the atropisomer structures move towards convergence with the TS structure as the TS is stabilized. Furthermore, F is able to propagate its effect towards the central C-C bond due to the stiffness of the aromatic rings; it is well known that stiff systems propagate forces more readily. The above properties are known for biaryl molecules, and form the basis of how F could predictably inform biaryl rotation. However, it would be useful to form a system of measuring the relationship between quantifiable parameters,

such as stiffness or π stacking interactions, and relate these to structural or behavioral changes. This would allow for a systematized approach to figuring out how F and τ might influence a novel system. In this way, large libraries of systems could be searched for parameters associated with a desired property or outcome imposed by F and τ application. In essence, it would be replacing intuition with a system of quantified parameters and outcomes, which provides the means to greatly expand the scope of systems that can be considered for mechanochemical control.

References:

1. F. Leroux, ChemBioChem 2004, 5, 644.
2. S. R. LaPlante, ChemMedChem. 2011, 6, 505.
3. L. Ma, C. Abney, W. Lin, Chem. Soc. Rev., 2009, 38, 1248.
4. S.R. LaPlante, P.J. Edwards, L.D. Fader, A. Jakalian, O. Hucke, ChemMedChem 2011, 6, 505.
5. F. Leroux, ChemBioChem 2004, 5, 644.
6. L. Pu, Chem. Rev. 1998, 98, 2405.
7. R. Noyori, H. Takaya, Acc. Chem. Res. 1990, 23, 345.
8. M.W.A. MacLean et al., Chem. Mater. 2014, 26, 5852.